

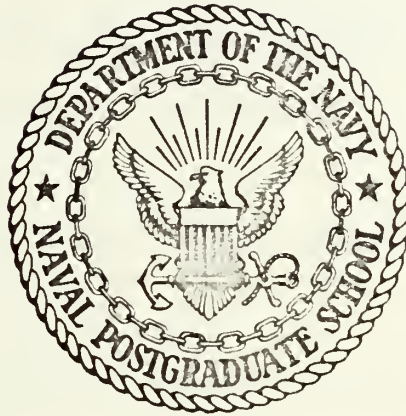
A METHOD FOR INCORPORATING NESTED  
FINITE GRIDS IN THE SOLUTION OF SYSTEMS  
OF GEOPHYSICAL EQUATIONS

Edward James Harrison



# NAVAL POSTGRADUATE SCHOOL

## Monterey, California



# THESIS

A Method for Incorporating Nested  
Finite Grids in the Solution of Systems  
of  
Geophysical Equations

by

Edward James Harrison, Jr.

Thesis Advisor:

R. L. Elsberry

June 1972

*Approved for public release; distribution unlimited.*



A Method for Incorporating Nested Finite Grids  
in the  
Solution of Systems of Geophysical Equations

by

Edward James Harrison, Jr.  
Lieutenant Commander, United States Navy  
B.S., Lehigh University, 1960

Submitted in partial fulfillment of the  
requirements for the degree of

DOCTOR OF PHILOSOPHY

from the

NAVAL POSTGRADUATE SCHOOL  
June 1972



## ABSTRACT

A numerical technique with simultaneous time integration of a meshed grid system is proposed, in which the fine mesh region is able to move within the coarse grid. The interface boundary conditions employed are shown analytically to be the only stable specification of those tested for a simple linear case. Numerical solutions using the meshed system are compared with those from uniform coarse and fine grids. One important criterion is that the solution within the fine mesh region of the meshed grid must have nearly the same accuracy as in a system which uses a fine mesh everywhere. The technique is applied to a two-dimensional  $(y,p)$  ten-level primitive equation model. Behavior of the meshed model is examined in experiments in which a small scale heat source is imbedded within an undisturbed zonal flow pattern. Energy boundary fluxes across the interface in the meshed system are shown to compare favorably with those in a uniform fine mesh grid. Three-dimensional  $(x,y,p)$  versions of the primitive equation model with single and multiple grid reductions are also examined. Simulated small scale disturbances are used to compare the meshed model solutions with those obtained on a uniform grid. Future applications of the meshing technique are suggested, such as in tropical storm research and general circulation models of the atmosphere and ocean.





## TABLE OF CONTENTS

I.	INTRODUCTION -----	6
II.	REVIEW OF MESHING TECHNIQUES -----	11
III.	THE MESHING TECHNIQUE AND BOUNDARY CONDITION EXPERIMENTS -----	17
	A. GENERAL CONSIDERATION -----	17
	B. COMPUTATIONAL STABILITY CONSIDERATIONS -----	18
	C. ANALYTIC AND NUMERICAL TESTS WITH OUTFLOW BOUNDARY CONDITIONS -----	23
	D. USE OF VARIABLE TIME INCREMENTS IN THE MESHED MODEL -----	35
IV.	ONE-DIMENSIONAL MOVEMENT EXPERIMENTS -----	41
	A. MOVEMENT OF THE FINE GRID -----	41
	B. LINEAR CASE -----	42
	C. NONLINEAR CASE -----	45
V.	TWO-DIMENSIONAL, NONLINEAR EXPERIMENTS -----	50
	A. THE PREDICTION MODEL -----	50
	B. TWO-DIMENSIONAL TESTS -----	52
	C. COMPUTATIONAL DEVICES USED IN THE MULTI-LEVEL MODEL -----	58
VI.	THREE-DIMENSIONAL EXPERIMENTS WITH A PRIMITIVE EQUATION MODEL -----	61
	A. THE PREDICTION MODEL -----	63
	B. INITIALIZATION OF THE MESHED GRID SYSTEM ---	67
	C. SR TEST 1: A SIMULATED TROPICAL STORM WITH DIABATIC HEATING -----	70
	1. Heating for the Tropical Storm Simulation (SR Model) -----	73
	2. Results of the SR Tropical Storm Simulation Case -----	78



D.	SR TEST 2: A TEST OF INITIALIZATION AND SIMULATED FRONTAL DEVELOPMENT---	88
VII.	THE MR MODEL: A MULTIPLE GRID INCREMENT REDUCTION -----	96
A.	THE GRID AND MARCHING PROCESS -----	96
B.	TROPICAL STORM SIMULATION IN THE MR MODEL---	100
VII.	SUMMARY -----	105
APPENDIX A	- SEMI DISCRETE AMPLIFICATION MATRICES FOR MESHED AND UNIFORM GRID SYSTEMS -----	112
LIST OF REFERENCES	-----	117
INITIAL DISTRIBUTION LIST	-----	120
FORM DD 1473	-----	123



### ACKNOWLEDGEMENT

I would like to thank Professor R. L. Elsberry, not only for his valuable assistance in this research, but also for his guidance in the development of my scientific viewpoint. I am also grateful to Professor R. T. Williams and Professor R. L. Haney for many helpful discussions and suggestions.



## I. INTRODUCTION

Use of nested finite grids in numerical applications has been studied by many authors in various disciplines. Although the approach may vary in the treatment of this subject, the ultimate goal is the same, namely higher resolution in specified areas of the grid network. The geophysical applications of such grid systems are many and varied. In atmospheric general circulation models, for example, higher resolution may be desirable over continental areas where orographic effects are important. Ocean models, on the other hand, often have continental boundary regions which require more careful consideration compared to the large scale flow. Atmospheric prediction models which are generally unable to adequately resolve such phenomena as fronts and tropical storms could incorporate fine mesh grids in these regions. There are several basic methods of approaching the limited area forecasting problem. The first method is to design a model in which a large enough geographic area is covered to permit boundary condition errors to be neglected. Except for the initialization, there can be no effect on the interior forecast by changes in the planetary scale flow with this technique. This, of course, limits the usefulness of such specifications to very short range forecasts. In addition, this method wastes both computer time and memory space. A second technique is to design a nested grid system in which the grid scale abruptly changes, and specifying the





required boundary values for the limited area grid from the larger scale forecast, or in some way assigning them from the interior at outflow points. It will be shown later that if equations on the grids are simultaneously integrated, there is a particular method of specifying boundary values at the interface that is computationally stable and produces a superior forecast.

There are, however, two other approaches to the problem of increased grid resolution in certain areas. The first of these involves the mathematical transform of a non-orthogonal, unequal spatial increment grid into a constant interval, orthogonal grid. Anthes (1970) has reported such a technique in which the non-orthogonal grid to be transformed had the property that the mesh size in both north-south (y), and east-west (x) directions varied smoothly from a minimum value at the center of the domain to a maximum value at the boundary. The equations were then transformed in terms of new independent variables on an orthogonal mesh, solved in the new system, and the results then transformed back to the original domain. Anthes showed that such a variable grid may be used in certain physical problems to gain resolution at the center of the grid over a limited time range. The major disadvantage of this type of formulation is the inability of the region of maximum resolution to move without moving the entire grid system. The small scale system of interest could well move a substantial distance from the high resolution area over the forecast period. Two computational



difficulties encountered with an analytic transformation are the loss of second order accuracy for centered space differencing, and the addition of non-linear terms resulting from the non-orthogonality of the transformed grid points in real space. Finally, one can retain orthogonality of a smoothly varying grid in one space dimension such as in axisymmetric hurricane models (Estoque 1962, Kuo 1965, Yamasaki 1968). Sundqvist and Veronis (1970) have shown that second order accuracy can be retained in a variable grid if the rate of variation is properly chosen. Since this technique does not apply to two-dimensional horizontal grids, it can only find application in a rather limited number of geophysical applications.

The systematic approach to the design of a nested grid system should begin with simple one-dimensional experiments with results which are applicable to more general systems, as opposed to the smoothly varying grid which is only applicable in one space dimension. Hence, one must evaluate the features which are desired in the nested system in general, and apply them in a simple case. The main problem is obvious, namely, the interface boundary condition of the nested system. In the first section of this report, it shall be shown analytically and with numerical integrations of a simple system, that only one of the types of boundary conditions tested can be specified when centered space and time differencing are used. This specification is computationally stable and leads to an accurate numerical solution. One-



dimensional numerical experiments show that many specifications which are computationally stable in uniform grid networks are extremely unstable in the meshed system. In the design of the system, one must also insure that the fine mesh grid (FMG) is able to move within the coarse mesh grid (CMG). This is necessary because it is desirable to have the smallest FMG possible to conserve computer time and memory space. The ultimate objective is to produce a forecast as accurate as that obtained on a grid which is fine mesh everywhere, but at a fraction of the computer cost. Thus, several one-dimensional tests, both linear and nonlinear, were performed to demonstrate this capability of the meshed system. Phase and amplitude errors are compared to those in uniform grid systems, and the meshed system is shown to compare favorably to the uniform fine grid.

A two-dimensional (y,p) primitive equation (PE) model was used in subsequent two-dimensional tests of the meshing technique. One of the primary objectives here was to study the boundary fluxes of kinetic and thermal energy through the interface. These fluxes could then be compared to those across the same region in a uniform fine grid. In these experiments, a localized heat source simulating a band of convective elements in an initially undisturbed flow was employed. Comparison of forecasts of various parameters were made between uniform coarse grids, uniform fine grids and the meshed grid model. In each case, the meshed system produced forecasts comparable to the uniform fine grid in the FMG



region, and superior to the uniform coarse grid outside this region.

Final tests of the meshing technique were made utilizing a four-level primitive equation model, suitable for conversion to possible operational uses with minimal changes. This model had two basic versions, one in which the grid scale changed abruptly from the coarse grid to the fine, and another in which the scale still changed abruptly, but in two steps. Thus, in the latter version, there were actually three different grid scales. Comparisons of uniform fine grid solutions were not possible for any of the three-dimensional cases because of computer memory and time limitations. Analytic initial states which simulated tropical storm and frontal scale disturbances were used in the comparisons of various aspects of the forecast fields. As in the two-dimensional model, realistic fluxes of kinetic and thermal energy were computed at the interface. Movement of the FMG while following the simulated disturbance had no apparent deleterious effects on the performance of the meshed system. Suggested future uses of the three-dimensional model are discussed as well as problems involving initialization of the FMG.





## II. REVIEW OF MESHING TECHNIQUES

One of the earliest applications of the concept of abruptly changing grid scales in a prediction model was made by Birchfield (1960). Utilizing the simple barotropic vorticity model, he showed improved trajectory forecasts of several tropical storms could be attained with a meshed grid system. The grid scale of the fine mesh grid in Birchfield's model was one-half that of the coarse mesh grid, and the fine mesh was initialized by interpolation from the CMG. One of the unique features of Birchfield's model was the simultaneous time integration of both grid scales. In the marching process, the vorticity equation was solved by relaxation techniques over the entire CMG. During this step, the presence of the FMG was ignored. After the CMG time step was complete, spatial and temporal interpolation of the tendencies at coincident points yielded boundary values for the subsequent FMG time steps. In each grid, the time increment was such that the stability criterion of Courant et al (1928) was satisfied. Thus, four time steps were taken in the FMG for every one in the CMG. Birchfield used one-fourth the time increment in the FMG because of the higher wind speeds in the storms. Interaction between scales was attained in this model by re-initializing the CMG after each time step, holding the FMG predicted value fixed at interior coincident points. This model, although one of the earliest meshed models, incorporated two very important features, namely



simultaneous time integration and a movable FMG. It will be shown later that simultaneous time integration on both grids is necessary for a stable, accurate forecast. Phillips (1972) also argued in favor of the "strategy" of simultaneous time integration.

Little concerning grid nesting techniques appeared in the literature until Howcroft's (1966) description of the proposed Air Weather Service's (AWS) fine mesh, barotropic vorticity model. The FMG spatial increment in the AWS model was again one-half that of the CMG. Initial data for the FMG were obtained by interpolation of geopotential heights at the time of Howcroft's report, however he noted that a fine grid analysis program was under development. The integration made use of a 24-hour forecast on a hemispheric coarse grid, retaining the appropriate coincident point values for use as boundary conditions in the subsequent FMG forecast. The fine mesh forecast was then carried out, updating the boundary values from the previous hemispheric forecast. This became a rather popular way of specifying boundary values for nested models, but it will be shown later that the method is generally unsatisfactory, even in linear models.

The need for detailed forecasts in active regions is reviewed in some detail by Bushby and Timpson (1967). They noted the important point that if fine mesh integrations are started from smooth realistic patterns of motion, temperature and humidity, obtained from large scale analysis, one may expect smaller scale detail to develop if the problem is



properly formulated. This is crucial for fine mesh models, for if it is not true, models with grid increments smaller than the distance between sounding stations have little meaning for operational forecasting. Bushby and Timpson's model was fine mesh everywhere, with the lateral boundary conditions specified from the interior of the forecast region. Such specifications will later be shown computationally unstable if not very carefully treated, and even in the stable cases may develop severe resonance. In a later report, Bushby(1968) noted that specification from the interior was in fact unsatisfactory, and that temporally constant lateral boundaries were adopted with an enhanced diffusion coefficient near the boundaries.

The use of independent large scale (hemispheric) forecasts to specify FMG boundaries was also used by Hill (1968) in the so-called "telescope" model. A numerical integration over an octagonal hemispheric grid was first carried out. Another grid with the same shape and number of points, but with half the grid spacing, was placed within the original grid, so that about one-quarter of the grid points coincided. The forecasts were generated separately, except for the boundary values for the FMG, which were obtained by spatial and temporal interpolation from the hemispheric forecast. The process may be repeated by placing a third grid within the second grid and so on. A later report concerning Hill's method by Shapiro and O'Brien (1970) proposed that a type of upstream difference be taken at outflow points, with the



previously discussed specification at the inflow points retained. This technique, originally suggested by Charney (1960), will be shown to be satisfactory, under certain conditions.

An important natural advantage of a fine mesh grid is the opportunity to portray the effects of the boundary layer in much greater detail. Horizontal variations due to features such as orography and boundary fluxes of heat and moisture can be simulated in a more realistic fashion as the grid scale begins to approach the scale of the phenomena themselves. A common feature in many operational prediction and general circulation models is the crude treatment of orographic features, particularly extensive mountain ranges such as the Alps, which have a profound effect on weather systems. Rosseau (1968), has reported on a meshed grid system developed for detailed local forecasts in the region of the Alps and Pyrenees. At some predetermined time ( $T$  hours before verification time) during the integration, the data of a hemispheric forecast in the region of interest was extracted from the forecast fields and interpolated to the FMG. This became the initial state for the regional forecast model over western Europe, which had a grid increment one-tenth that of the hemispheric model. Very detailed orography was modeled to produce regional forecasts for France during the FMG integration over the  $T$  remaining hours. Rosseau noted that extracting boundary values from the subsequent independent hemispheric forecast led to severe computational noise,





which masked meteorological development. As a consequence, Rosseau formulated outflow boundary conditions based on the upstream differencing of the potential vorticity, as suggested by Charney (1960). The major disadvantage of this specification is the lack of interaction between the grid scales. Due to the greatly increased computer time and memory space required for such a fine grid, this integration was only for three hours for one data set, making evaluation difficult.

Another approach to the limited area forecasting problem was that by Gerrity and McPherson (1969). In this barotropic primitive equation (PE) model, the integration was carried out on a uniform fine grid mainly covering the North American continent. The grid spacing for this model was about 190 km at 60N, or one-half that of the National Meteorological Center (NMC) hemispheric model. The boundary values were temporally constant, and Euler "backward" differencing was used throughout. Since the "semi-momentum" (Shuman and Hovermale 1968) space differencing was used, as well as external smoothers, it is difficult to determine the effects of the temporally constant boundary values in this model. It is clear, however, that such a model is useful only for very short range forecasts in regions well away from the boundary.

Wang and Halpern (1970) reported experiments with a barotropic PE model similar to that just described. The spatial differencing was the same, but the boundary conditions were obtained from an independent CMG forecast, and



leapfrog-trapezoidal (Kurihara 1965) time differencing was employed. External smoothers were also employed to remove the noise inherent in the boundary specification. The major disadvantage was absence of interaction between grid scales. A more sophisticated use of the barotropic primitive equation model was made by Ookochi (1972), in which he employed simultaneous time integration on both scales. This model was solved on a staggered grid using Euler backward time differencing, and a spatial averaging technique to describe the boundary conditions at the interface between grid scales. Ookochi experimentally showed the method to be computationally stable over the period of integration, but the model does not include the type of gravity waves discussed by Phillips (1972). Another disadvantage was the lack of provision for moving the fine grid region, resulting in distortion of phase speed as relatively short waves passed from one grid to the other.



### III. THE MESHING TECHNIQUE AND BOUNDARY CONDITION EXPERIMENTS

#### A. GENERAL CONSIDERATION

The most obvious problem in a nested grid system is the treatment of the interface between the two scales. Mathematical treatment of a similar problem was given by Osher (1970) for solution of the heat diffusion equation on a grid with an abrupt spatial increment change. Appropriate difference equations were shown to be maximum norm stable over the whole spatial domain, and particularly at the interface. Ciment (1971) examined the solution of the linear equation

$$\frac{\partial u}{\partial t} = - U \frac{\partial u}{\partial x} \quad (1)$$

across a discontinuity in grid spatial increment and showed certain dissipative differencing schemes such as the Lax-Wendroff, are stable approximations to (1) over the whole domain. It will be shown that under certain conditions, the centered space and time differencing commonly used in meteorological models is also a stable approximation. Treatment of the outflow boundary for (1) has been studied by many authors. Outflow boundaries are particularly troublesome when centered spatial differencing is used due to possible separation of the solution at alternate grid points. Platzman (1954) showed that, in general, the outflow boundary value should be externally specified, although there are certain cases which allow a specification from the interior. Many possible outflow boundary specifications have been



examined in numerical tests by Nitta (1962), who, however, did not include a test in which the exact solution was specified on the outflow boundary. It will be shown later that not only is this specification computationally stable, but yields an accurate numerical solution for low wave numbers. Since this specification is possible for only very simple cases, one may argue heuristically that specifying a numerical solution from a larger grid at the outflow point might also give good results. In the nested system, the problem is compounded, as outflow boundaries for both grid scales must be considered.

#### B. COMPUTATIONAL STABILITY CONSIDERATIONS

Three basic grids were employed for the linear tests to demonstrate the meshing technique and compare various boundary specifications. The first grid was a uniform mesh control which merely specified cyclic continuity of the periodic initial state. Numerical solutions of (1) on such a grid are thus free of boundary conditions, and if the stability criterion of Courant et al (1928) is met, the solution cannot become contaminated by computational noise. This grid was identical to the CMG grid in the meshed model, and direct comparisons of numerical solutions were made. Thus, the only factor which could possibly have caused differences was the presence of the FMG. The second grid system utilized was similar to that of Nitta (1962), wherein the exact solution is specified at the inflow, while various outflow conditions may be tested in the numerical solution of (1).





This grid, which was thus quite different from the nested model which was cyclic, was very convenient in the outflow condition tests. The third grid was, of course, the meshed grid system, an example of which is depicted in Figure 1.

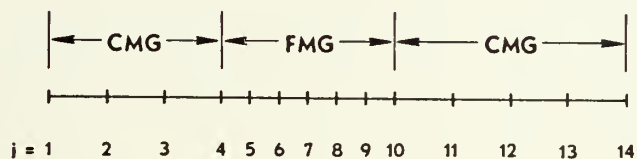


Fig. 1. Meshed grid for  $p = 2$ . The CMG is cyclic, and for this example, the FMG covers three CMG intervals.

Note that the grid abruptly changes spatial increment at the points  $j = 4$  and  $j = 10$ . An integer  $p$  is defined, which is the ratio of the spatial increment ( $\Delta x_2$ ) in the CMG to the increment ( $\Delta x_1$ ) in the FMG.

An approach similar to that of Platzman (1954) was utilized for the meshed model, to demonstrate computational stability of a certain interface boundary specification which will henceforth be called "mutually determined." The mutually determined boundary condition is specified in the following manner. In Figure 1, for example, the solution domain of the FMG is defined to be from  $j = 4$  to  $j = 10$ , and the CMG domain from  $j = 1$  to  $j = 6$ , and from  $j = 8$  to  $j = 14$ . Thus, there is an overlap of the solution domains of one CMG grid increment. In the simultaneous time



integration, the solution at the points  $j = 4$  and  $j = 10$  in Figure 1 is determined by the CMG, while at  $j = 6$  and  $j = 8$ , the solution is on the FMG. In this fashion, a dual initial-boundary problem may be solved with simultaneous time integration. Because the solution from each grid is used to determine boundary conditions for the other, mutual interaction can occur across the interface. There are, of course, other specifications which may be utilized at both ends of the FMG, but for the following tests, only the FMG outflow boundary was modified. On the inflow point, the mutually determined condition was retained. The main point of these tests was to show that the only computationally stable specification of those tested for the outflow boundary of the FMG was the mutually determined condition.

Approximating the spatial derivative of (1) with a centered difference, but keeping time as a continuous variable, yields the following non-dimensional, "semi-discrete" difference equation

$$\frac{\partial u}{\partial \tau} = \frac{1}{2} (u_{j+1} - u_{j-1}) \quad (2a)$$

in the CMG, and

$$\frac{\partial u}{\partial \tau} = \frac{1}{2p} (u_{j+1} - u_{j-1}) \quad (2b)$$

in the FMG, where  $\tau = -\frac{Ut}{\Delta x_2}$ . The external boundaries of the CMG are cyclic, so that any contamination of a numerical solution must arise at the interface. The point  $j = 10$  is thus the outflow boundary for the FMG if it is assumed that  $U > 0$  in (1), and various boundary conditions were specified



here. At the outflow point for the FMG ( $j = 10$  in Figure 1) the mutually determined condition is

$$\frac{\partial u_{10}}{\partial \tau} = \frac{1}{2} (u_{11} - u_8)$$

in the CMG, where  $u_8$  is calculated on the FMG, and

$$\frac{\partial u_8}{\partial \tau} = \frac{1}{4} (u_{10} - u_8)$$

in the FMG. The mutually determined condition at the inflow point  $j = 4$  is

$$\frac{\partial u_4}{\partial \tau} = \frac{1}{2} (u_6 - u_3)$$

in the CMG and

$$\frac{\partial u_5}{\partial \tau} = \frac{1}{4} (u_6 - u_4)$$

in the FMG. The system of difference equations over the whole spatial domain for this simple linear example may be expressed by the matrix equation

$$\frac{\partial u}{\partial \tau} = \tilde{A}u \quad (3)$$

where  $u = \text{col } (u_1, u_2, \dots)$ .

and

$$\tilde{A} = \frac{1}{2} \begin{pmatrix} 0 & 1 & 0 & 0 & 0 & 0 & 0 & 0 & 0 & 0 & 0 & 0 & 0 & -1 \\ -1 & 0 & 1 & 0 & 0 & 0 & 0 & 0 & 0 & 0 & 0 & 0 & 0 & 0 \\ 0 & -1 & 0 & 1 & 0 & 0 & 0 & 0 & 0 & 0 & 0 & 0 & 0 & 0 \\ 0 & 0 & -1 & 0 & 0 & 1 & 0 & 0 & 0 & 0 & 0 & 0 & 0 & 0 \\ 0 & 0 & 0 & -0.5 & 0 & 0.5 & 0 & 0 & 0 & 0 & 0 & 0 & 0 & 0 \\ 0 & 0 & 0 & 0 & -0.5 & 0 & 0.5 & 0 & 0 & 0 & 0 & 0 & 0 & 0 \\ 0 & 0 & 0 & 0 & 0 & -0.5 & 0 & 0.5 & 0 & 0 & 0 & 0 & 0 & 0 \\ 0 & 0 & 0 & 0 & 0 & 0 & -0.5 & 0 & 0.5 & 0 & 0 & 0 & 0 & 0 \\ 0 & 0 & 0 & 0 & 0 & 0 & 0 & -1 & 0 & 0 & 1 & 0 & 0 & 0 \\ 0 & 0 & 0 & 0 & 0 & 0 & 0 & 0 & -1 & 0 & 1 & 0 & 0 & 0 \\ 0 & 0 & 0 & 0 & 0 & 0 & 0 & 0 & 0 & -1 & 0 & 1 & 0 & 0 \\ 0 & 0 & 0 & 0 & 0 & 0 & 0 & 0 & 0 & 0 & 0 & -1 & 0 & 1 \\ 1 & 0 & 0 & 0 & 0 & 0 & 0 & 0 & 0 & 0 & 0 & 0 & -1 & 0 \end{pmatrix}$$

where the first and last rows reflect the cyclic continuity



in the CMG. The factor .5 appears in the equations for the FMG because the space increment is one-half that of the CMG for this example. The fourth and tenth rows indicate the CMG difference equations at  $j = 4$  and  $j = 10$  respectively, while the adjacent interior rows represent the FMG difference equations at  $j = 5$  and  $j = 9$ .

The matrix equation (3) is a matrix differential equation of the first order, with the fundamental solution  $\exp \tilde{A}t$ . If the eigenvalues of  $\tilde{A}$  are  $\lambda_k$ ,  $k = 1, 2, \dots$ , then the fundamental modes of  $u$  are  $\exp \lambda_1 t$ ,  $\exp \lambda_2 t, \dots$ . These semi-discrete modes will then amplify or damp if the real parts of the  $\lambda_k$  are positive or negative, respectively. If the eigenvalues have no real parts, the semi-discrete modes are neutral. Platzman (1954) has shown that if any of the semi-discrete modes either amplify or damp, then the modes of the fully discrete system

$$u_j^{n+1} = u_j^{n-1} + \Delta \tau (u_{j+1}^n - u_{j-1}^n) \quad (4a)$$

in the CMG, and

$$u_j^{n+1} = u_j^{n-1} + \frac{\Delta \tau}{2} (u_{j+1}^n - u_{j-1}^n) \quad (4b)$$

in the FMG, will amplify exponentially. This was defined as the "secondary" stability criterion by Platzman (1954), as opposed to the "primary" criterion developed by Charney et al (1950), which requires that the magnitude of the maximum eigenvalue of the fully discrete amplification matrix be equal to, or less than unity. The eigenvalues of  $\tilde{A}$  may be obtained numerically, and for this case, all the





eigenvalues of  $\tilde{A}$  were pure imaginary numbers. Thus, in the fully discrete integration of (1) with centered space and time differencing, one may expect no exponential growth due to the boundary specification. To further illustrate this stability for the meshed system, the fully discrete amplification matrix may be obtained in the following manner. In (4), define a new variable  $w_j^n$  such that

$$w_j^n = u_j^{n-1}, \quad w^{n+1} = u^n$$

The fully discrete system may now be written

$$\tilde{W}^{n+1} = \tilde{B} \tilde{W}^n$$

where for the example in Figure 1

$$\tilde{W} = \text{col} (w_1, w_2, w_3, \dots, u_1, u_2, \dots)$$

and

$$\tilde{B} = \begin{pmatrix} \tilde{0} & \tilde{I} \\ \tilde{I} & \tilde{A} \end{pmatrix}$$

where  $\tilde{I}$  is the identity matrix and  $\tilde{0}$  is the zero matrix. Again, the eigenvalues for  $\tilde{B}$  were numerically determined, with the largest magnitude equal to 1.0000. Thus, the stability criterion derived from the semi-discrete system is also demonstrated for the fully-discrete case.

### C. ANALYTIC AND NUMERICAL TESTS WITH OUTFLOW BOUNDARY CONDITIONS

The semi-discrete stability analysis was then applied to several other specifications in the meshed model, as well as in a uniform grid system. For specifications involving



more than one time level, such as the upstream differencing, and for external specifications, numerical tests using centered space and time differencing were performed. Table 1 summarizes the results of these tests. In the listing of specifications in Table 1, the outflow point index is  $j$ , while  $n = 0, 1, 2, \dots$  is the time level for the integration of the fully discrete system (4). For the numerical tests, the simple initial state was a sinusoid of wave number 1 on the one-dimensional grid of unit non-dimensional length. In Table 1,  $t'$  is defined in the usual manner where  $x = Lx'$ , and  $t = L/U t'$ , if the scale of  $u$  is  $U$  in (1). The one-dimensional grid utilized a CMG spatial increment of 0.01 non-dimensional units and an FMG increment of 0.005 non-dimensional units. In the uniform grid, the spatial increment was the same as that in the CMG, and a time increment of 0.0025 non-dimensional units was used for all cases, regardless of the spatial increment of the grid. Later in this section, we examine the behavior of the "stable" specifications with initial states involving higher wave numbers. The various semi-discrete amplification matrices for the cases in Table 1 may be found in Appendix A. There is not a one-to-one correspondence between the magnitude of the largest real eigenvalue in Table 1 and the time at which exponential growth of the solution initiated because of the large number of computational modes for each solution.

Specification 1 (mutually determined) is, of course, not applicable to the uniform grid, and as seen earlier, no



Table 1

Summary of outflow boundary tests

<u>No.</u>	<u>Outflow Specification</u> <sup>1</sup>	<u>Largest Eigenvalue</u> <sup>2</sup>		<u>Critical Time</u> <sup>3</sup>	
		<u>Uniform Grid</u>	<u>Meshed Grid</u>	<u>Uniform Grid</u>	<u>Meshed Grid</u>
1	Mutually determined	-	0.0000	-	stable
2	Independent CMG	-	-	-	stable
3	$u_j^{n+1} = \sin 2\pi[(j\Delta x) - (n+1)\Delta\tau]$	-	-	stable	2.5
4	$u_j^{n+1} = u_j^0$	0.0000	0.1269	stable	2.8
5	$u_j^{n+1} = u_{j-1}^{n+1}$	1.0000	0.2423	2.9	1.1
6	$u_j^{n+1} = u_{j-2}^{n+1}$	0.0000	0.1332	stable	1.8
7	$u_j^{n+1} = 2u_{j-1}^{n+1} - u_{j-2}^{n+1}$	1.5000	0.3565	2.8	1.9
8	$u_j^{n+1} = u_j^n + \frac{\Delta\tau}{\Delta x}(u_{j-1}^n - u_j^n)$	-	-	stable	2.5

<sup>1</sup>See text for explanation.<sup>2</sup>Largest real part of the maximum eigenvalue of the semi-discrete amplification matrix when such matrix is defined.<sup>3</sup>Non-dimensional time at which exponential growth began in the fully discrete numerical integration.



instabilities arise from this interface condition. The numerical solution for this specification after 4000 time steps ( $t' = 10$ ) is depicted in the upper portion of Figure 2, compared with the exact solution. The location of the stationary FMG is denoted by the vertical dashed lines in Figure 2.

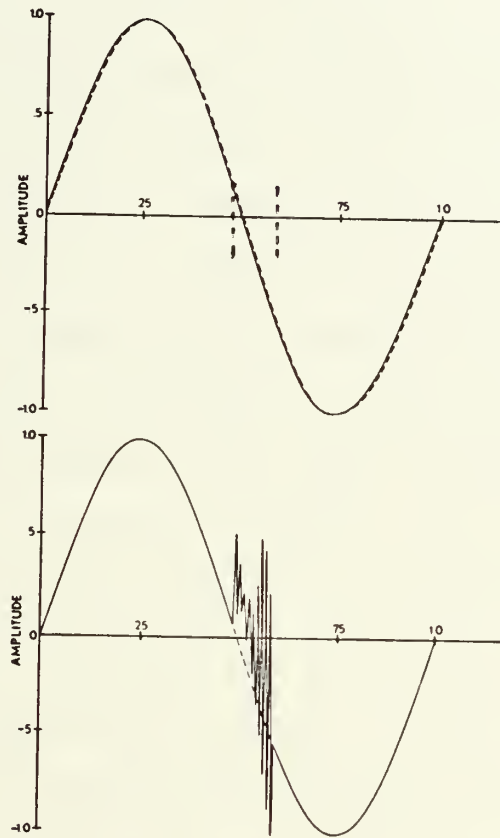


Fig. 2. Numerical (solid) and exact (dashed) solutions at  $t' = 10$  for specification 1 (upper) and specification 2 (lower). See text and Table 1 for details.

The solution exhibited no computational noise, amplitude was conserved to within 0.01 percent, and only a small phase error occurred for this relatively long wave. This may be compared to the solution portrayed in the lower portion of





Figure 2, which results when an independently integrated CMG (specification 2 in Table 1) is used to specify the boundary values of FMG. This non-simultaneous solution corresponds to the approach of solving the equations on a coarse grid first, independent of the fine grid. The appropriate coincident point values are retained for use as boundary values in the subsequent FMG integration. As the solutions on the different grids diverge, slight inconsistencies in the FMG boundary values quickly fill the forecast region with computational noise. Because this is essentially an external specification, no exponential growth of the computational modes occurred, in fact, amplitude was conserved to within two percent. As seen in Figure 2, however, the solution is so contaminated that even the use of heavy smoothing would not render it usable. In a nonlinear model, this computational noise would lead to aliasing, and possibly to nonlinear computational instability. Phillips (1972) has shown, using the method of characteristics, that the independently integrated CMG specification can probably not be applied in a general multi-level model. In simple barotropic models, which do not allow internal gravity waves, phase speed magnitude of external gravity waves is always greater than the advective speed, but in multi-level primitive equation models, values of internal gravity wave propagation speed will be encountered for short vertical wavelengths which are less than the advective speed. For this case, Phillips showed that no external specification should



be made from the coarse grid unless (perhaps) these values have been determined by a numerical method in which they are suitably affected by the fine mesh calculation.

Specification 3 (exact solution) is a purely external specification, and is, therefore, computationally stable in the uniform grid. Figure 3 portrays this numerical result for the long wave case, and except for the "stair step" noise, the solution was qualitatively quite good. This is the first example of a specification which was stable in the uniform grid, but quite unstable in the meshed system. Computational noise initiated by slight inconsistencies between the numerical solution and specifications 3 - 8 in Table 1 propagated upstream through the FMG in the meshed model. In

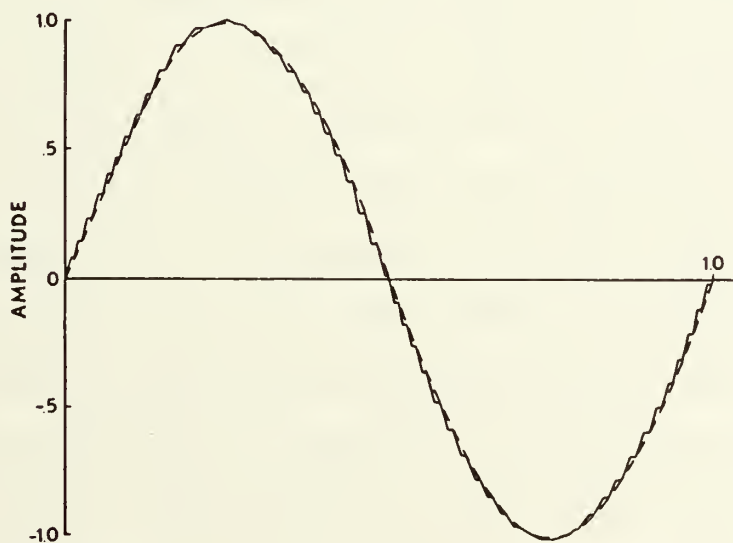


Fig. 3. Numerical solution (solid) compared with exact solution (dashed) as  $t' = 10$  for specification 3. See text and Table 1 for details.



the uniform grid system, this noise was reflected in a stable manner by the inflow boundary, and does not cause exponential growth of these modes. However, in the meshed system, the computational modes represented an erroneous solution at the interface and thus contaminated the CMG solution, since the inflow of the FMG is the outflow for the CMG. The upper portion of Figure 4 depicts the behavior of the natural logarithm of system amplitude squared versus time during the integration for specification 3 in both models. The solution in the meshed system remained stable until the computational modes reached the other interface boundary. At approximately  $t' = 2.5$  (see Figure 4), the amplitude began to grow exponentially in the meshed model, while the solution in the uniform grid was accurate.

Specification 4 (constant in time) was shown by Platzman (1954) to be computationally stable in a uniform grid, and this is verified in Table 1. The lower portion of Figure 4 depicts the behavior of this solution for both uniform and meshed models. Because this specification is extremely inconsistent with the numerical solution, large amplitude computational modes were generated at the outflow boundary, and quickly filled the entire forecast region. The computational modes grew linearly in the uniform grid model, and very quickly exponentially in the meshed system. Nitta (1962) mistakenly concluded that this boundary condition led to exponential growth in a uniform grid, but this was probably because his integrations were not carried out far



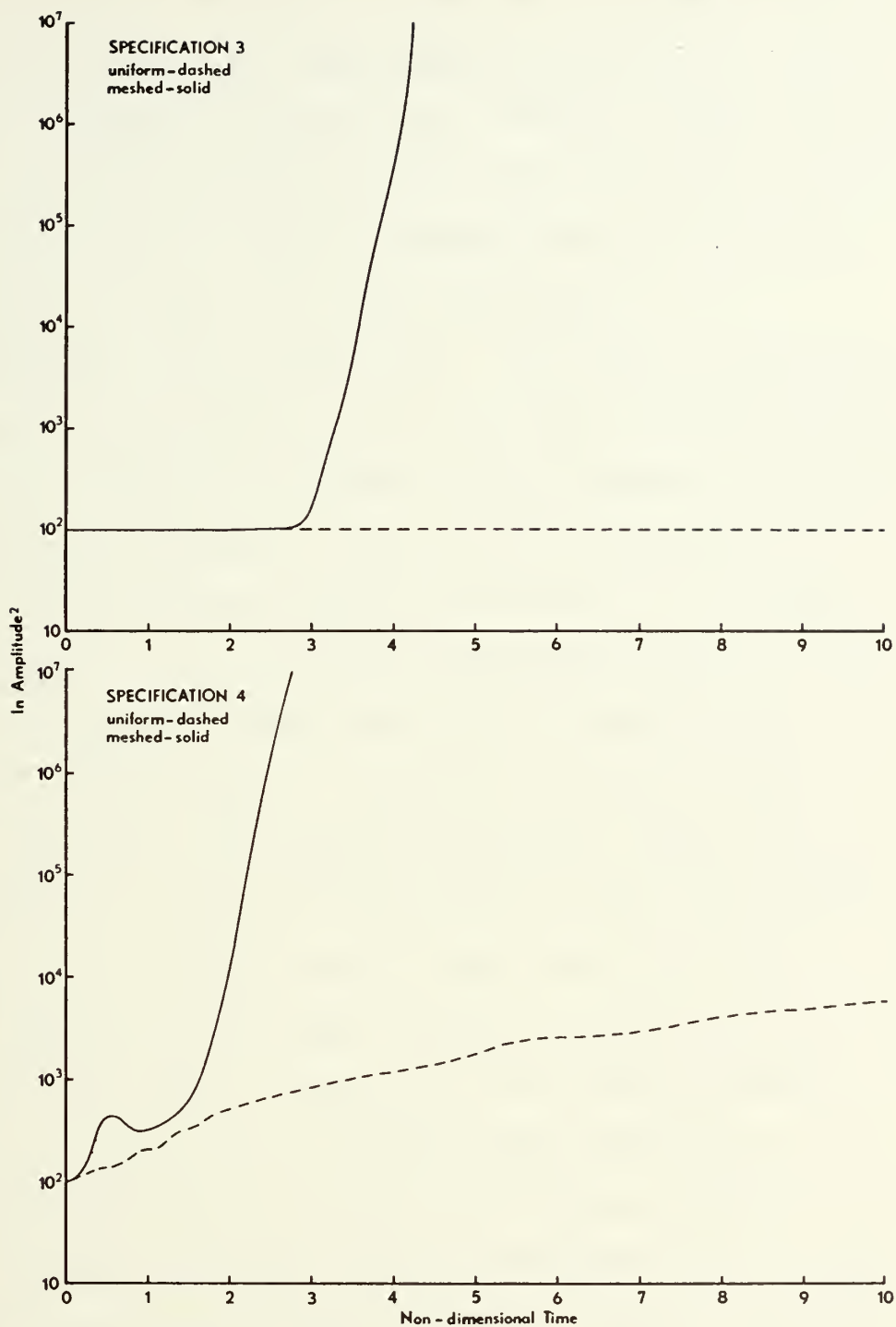


Fig. 4. Natural logarithm of system amplitude squared vs. non-dimensional time for specification 3 (upper) and specification 4 (lower). See text and Table 1 for details.





enough in time. One must be cautious in drawing conclusions from purely numerical experiments in which only a short integration period is considered. Platzman (1954) has shown that exponential growth does not occur with such external specifications, and this is demonstrated by the linear growth depicted in Figure 4 for the uniform grid.

Assigning the outflow point the value of the adjacent interior point (specification 3) excites rapid exponential growth of computational modes in both models, as portrayed in the upper portion of Figure 5, and indicated by the real part of the maximum eigenvalue in Table 1. It should perhaps be noted that each unstable specification listed in Table 1 had many unstable modes, but only the maximum real part was listed in this report. The lower portion of Figure 5, however, indicates that entirely different behavior took place in the uniform grid when the outflow point was assigned the value of the second interior point (specification 6). The modes amplified and damped quasi-periodically with no net growth, and this is indicated by the purely imaginary eigenvalues for this case. Computational stability for this specification is a result of the centered spatial differencing, in that the finite spatial difference at the first interior point was zero for all time. Spatial separation at alternating grid points is thus unable to affect the outflow boundary, as in the previous specification. The numerical solution, while computationally stable, is obviously useless.



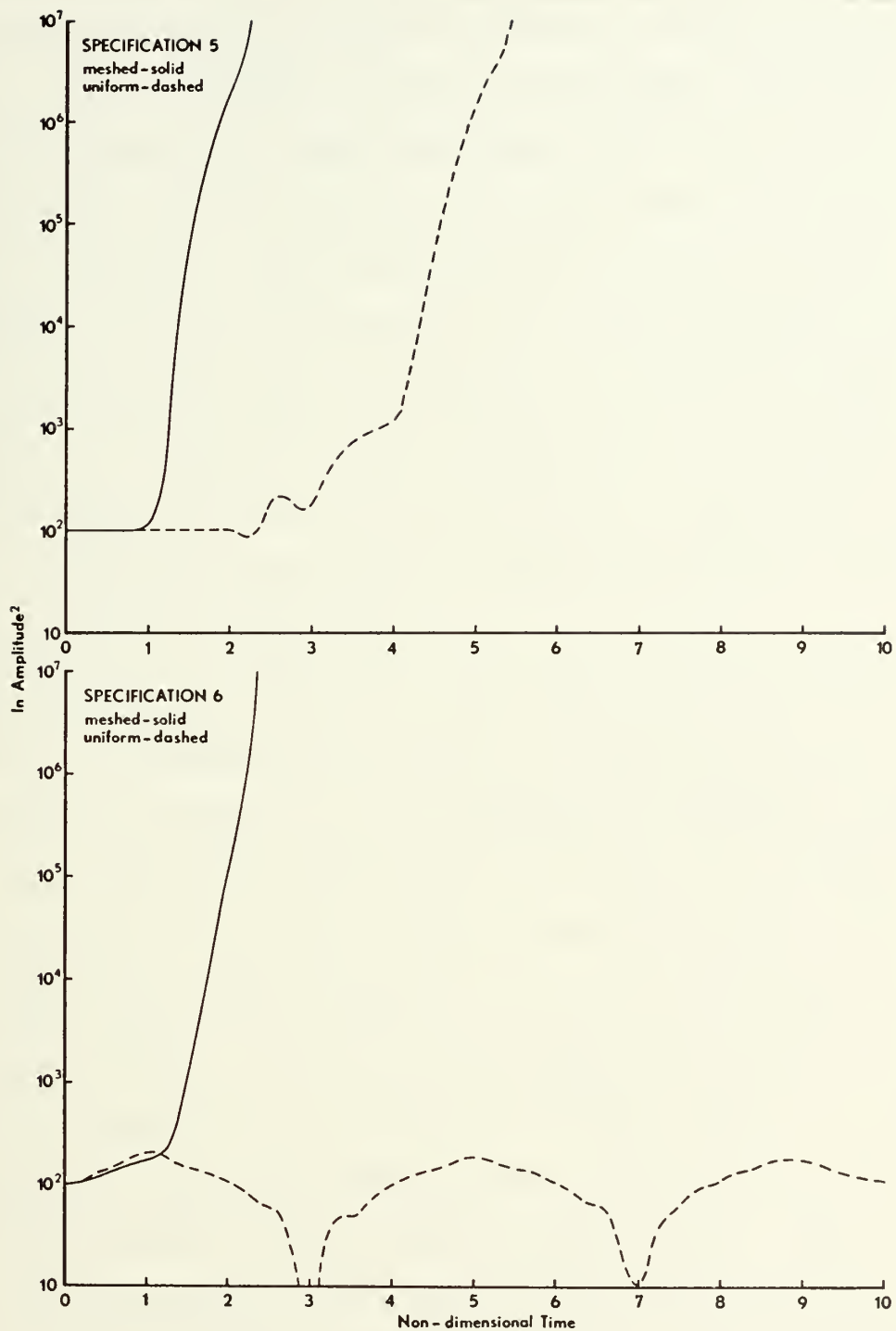


Fig. 5. Natural logarithm of system amplitude squared vs. non-dimensional time for specification 5 (upper) and specification 6 (lower). See text and Table 1 for details.



Specification 7, on the other hand, in which the value at the outflow point is obtained by linear extrapolation from the two adjacent interior points, is strongly affected by the solution separation. Once initiated, rapid exponential growth occurs in both systems as can be seen in the upper panel of Figure 6. As noted earlier, one may be misled into concluding that the specification is computationally stable simply because the solution remains accurate for a short integration. As may be seen in Figure 6, the solution conserves amplitude, and is quite accurate in the uniform grid for some time, but the onset of exponential growth is sudden, and the growth is explosive.

The last case treated in these experiments was the utilization of an upstream difference at the outflow point (specification 8) similar to that suggested by Charney (1960). This is a dissipative differencing scheme (e.g., forward in time, backward in space), and in combination with centered space and time differencing at all other grid points, gave excellent results. This is also essentially the same specification suggested by Shapiro and O'Brien (1970) for Hill's "telescope" model discussed earlier. Hill used an independent CMG forecast to obtain FMG boundary values (specification 2), and Shapiro and O'Brien showed that the use of upstream differencing at outflow boundaries led to superior results. In the simultaneous integration of the meshed system, however, this specification also led to eventual exponential growth of the computational modes as seen in the lower portion of Figure 6.



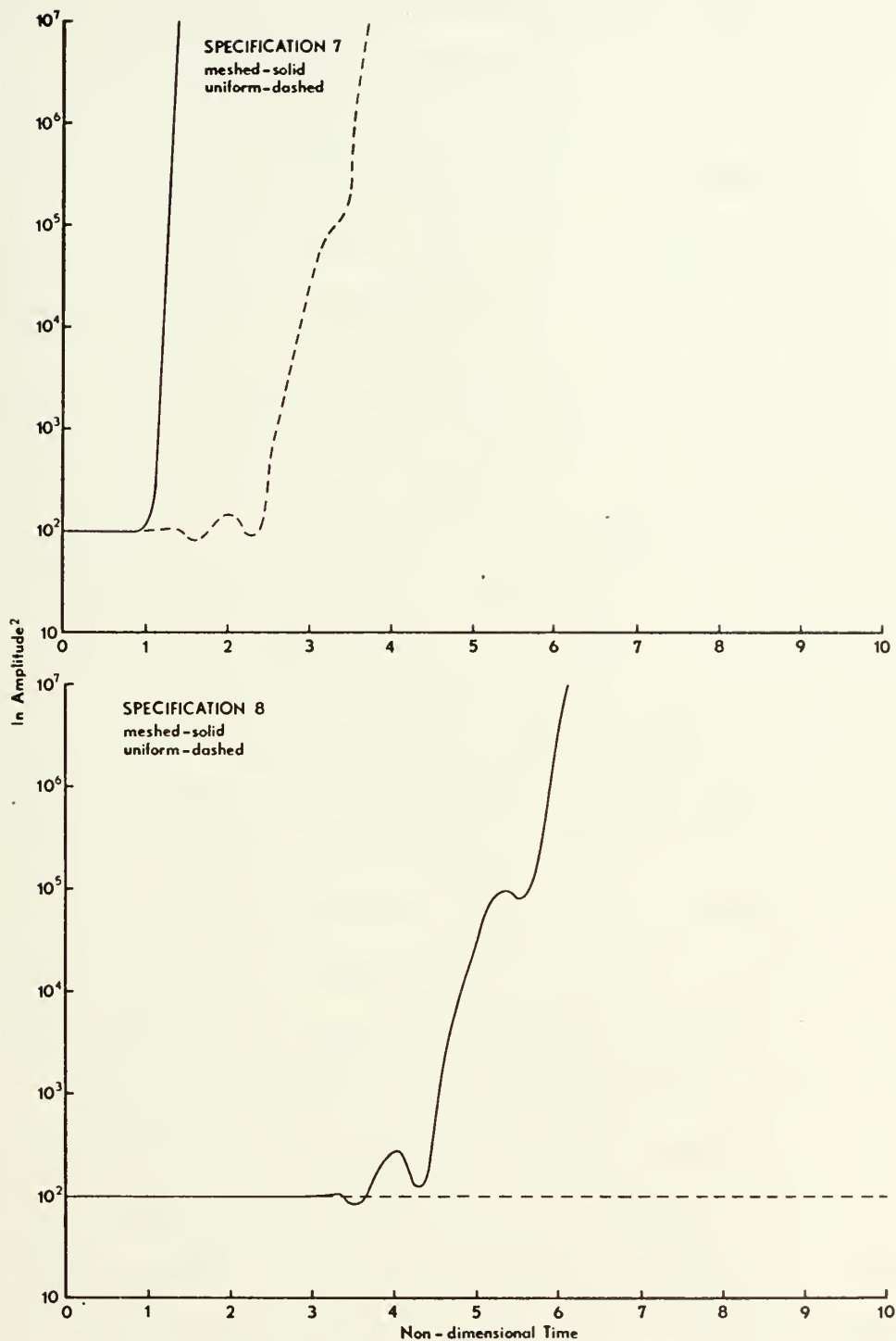


Fig. 6. Natural logarithm of system amplitude squared vs. non-dimensional time for specification 7 (upper) and specification 8 (lower). See text and Table 1 for details.





#### D. USE OF VARIABLE TIME INCREMENTS IN THE MESHED MODEL

The stability analysis described in the previous section is valid only when the FMG is stationary and the same value of the time increment ( $\Delta t'$ ) is used in the numerical integration of (4) in both grids. Use of a sufficiently small time increment to satisfy the Courant et al (1928) stability requirement in the fine grid not only reduces the accuracy of the solution in the CMG, but partly defeats one of the objectives of the meshed model, namely to reduce the computation time compared to a grid which is everywhere fine mesh.

The next series of tests, therefore, were exactly the same as those discussed in the previous section, except that the time increments were in the same ratio as  $p$ , and higher wave numbers were used. Only those specifications which were computationally stable and produced accurate results were tested in this section. Thus, for the meshed model, only specification 1 (mutually determined) was used, and for the uniform grid model, only specifications 3 and 8 (exact value and upstream differencing) were tested. The results for the uniform grid were, of course, as previously discussed, and the solutions for wave number one (not shown) closely resembled the upper portion of Figure 2. The meshed system was tested for  $p = 2$  and  $p = 5$ , and also yielded a very accurate solution for both cases for wave number one. This was an extremely important result, as it verified the tacit assumption of linearity over the CMG time interval.



The FMG value at the external interface ( $j = 4$  and  $j = 10$  in Figure 1, for example) was determined after each FMG time step by linear temporal interpolation of the CMG solution for the tendency at this point. That is, the marching process required that the CMG time step be taken first, then the tendency at each FMG external boundary applied after each FMG time step.

Higher wave number sinusoids were then imposed as the initial state to determine the behavior of the meshed grid when larger gradients passed through the stationary interface region. The first test was for an initial state of wave number two. The meshed model numerical solution for  $p = 5$  after 4000 time steps is compared to the exact solution in Figure 7. Amplitude is predicted accurately, but

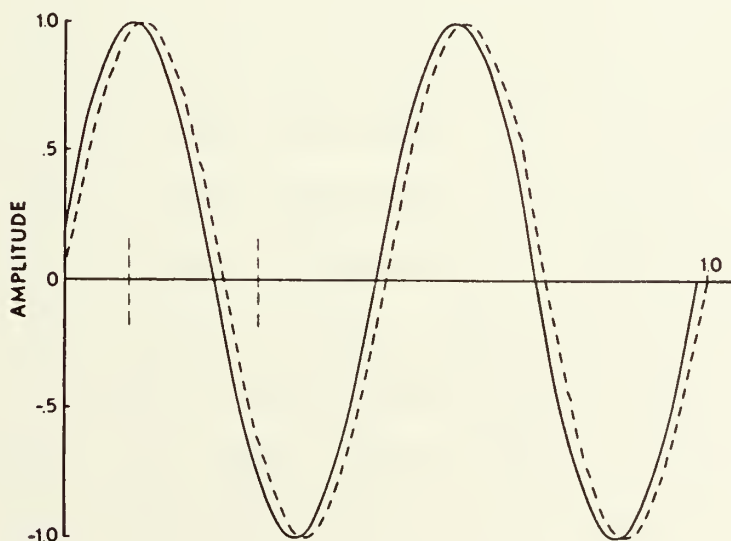


Fig. 7. Numerical solution (solid) compared with exact solution (dashed) for the meshed system with  $p = 5$ . The location of the FMG is denoted by the vertical dashed lines. For this test the FMG was stationary.



the phase error is approximately 0.03 wavelengths. The solutions for  $p = 5$  were slightly more accurate than those for  $p = 2$  (not shown) in every case, suggesting that higher values of  $p$  yield more accurate solutions over the entire grid. It will be shown later in nonlinear cases that the presence of the FMG in the model over strongly perturbed areas significantly improved the solution over the entire prediction domain, compared to a uniform coarse grid system. The uniform grid solution with the exact value specified at the outflow point (specification 3) for the wave number two case became extremely contaminated by computational noise, and hence it was eliminated from further tests. The upstream difference (specification 8), on the other hand, produced an extremely accurate solution over the uniform grid with virtually no error in either amplitude or phase for wave number two.

The grid systems were then compared for the numerical solution of (4) when wave number four was imposed as an initial state. These solutions are compared in Figure 8, with the meshed model solution in the upper panel, and the uniform grid solution in the lower portion. The meshed grid solution in Figure 8 shows that the solution is accurate for the amplitude, but with a phase error of nearly 0.25 wavelengths after 4000 time steps. This result may be compared to the control run, which was exactly the same grid without the FMG (cyclic continuity), where the phase error was slightly greater than that of the meshed system (not shown).



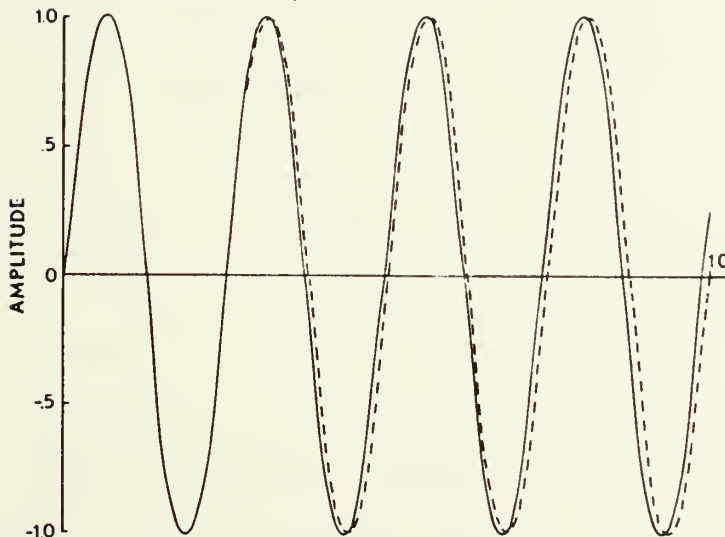
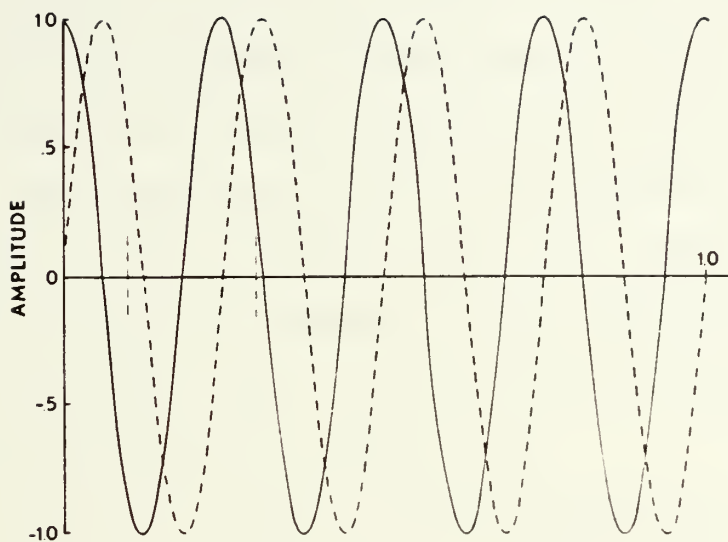


Fig. 8. Numerical (solid) compared with the exact solution (dashed). The upper panel depicts the comparison for the meshed system for wave number four with the location of the FMG denoted by the vertical dashed lines. The lower panel depicts the same comparison for a uniform coarse grid with specification 8 as an outflow condition, and the exact value as an inflow condition.





This result suggested that the presence of the FMG will not significantly improve the phase speed forecast of short wavelength features if they are allowed to pass through the interface. This is obviously a strong argument for a non-stationary FMG which could remain centered over the short wavelength feature. The improvement of the phase speed solution in the meshed system over the control run was in approximately the same ratio as  $p$ . For example, if the FMG covered one-fifth of the total grid, then the phase error was approximately one-fifth less than the control run.

The upstream difference (specification 8) yielded a relatively accurate solution, free of computational modes as may be seen in the lower panel of Figure 8. This solution cannot actually be compared to the one above it, because the exact value was specified at the inflow at each time step, but is shown mainly to demonstrate that this specification leads to good results, even with relatively short wavelength features. The result indicates that for uniform grids with centered space and time differencing, the upstream difference should be used at outflow points. This is in agreement with similar findings by Charney (1960) and Shapiro and O'Brien (1970). Further boundary condition tests with uniform grid, limited area models should be made, using nonlinear equations. One major disadvantage of the upstream specification is that system energy may not be conserved. For very short range forecasts over limited areas, however, rather elaborate energy conserving boundary specifications and difference



schemes such as those proposed by Elsberry and Harrison (1971) may not be necessary. This was also suggested by Bushby and Timpson (1967) for limited area fine grid models.



#### IV. ONE-DIMENSIONAL MOVEMENT EXPERIMENTS

##### A. MOVEMENT OF THE FINE GRID

In general, the large scale flow has relatively small gradients of the dependent variables except in strongly perturbed regions. The results in the last section strongly indicated that to prevent large phase errors for short wavelength, large amplitude features, one should not allow such features to pass through the interface into the CMG. Hence, the FMG must be large enough to completely encompass the region of interest within the internal interface boundaries, and must be able to move in the appropriate direction if the feature approaches the interface. The movement tests showed that the meshed system satisfied two important criteria, namely that the solution remain computationally stable, and that it has comparable accuracy to that obtained on a uniform fine grid.

If the movement criteria, perhaps a region of large gradient approaching the interface was met, the FMG was moved one CMG spatial increment in the appropriate direction. This movement required new FMG values on the leading edge at both FMG time levels, and new CMG values on the trailing edge at both CMG time levels. It should be noted that the required previous time levels for the two grids are not temporally coincident. The trailing edge CMG values are simply assigned those of the previously spatially coincident FMG



points. Those at the current time level present no problem, but those for the previous CMG time level correspond to values from  $p$  previous time steps in the FMG. This time "alignment" is also a problem on the leading edge. On the leading edge, new values were obtained by first spatially interpolating the CMG values at both CMG time levels. The values were then interpolated in time to obtain previous time step FMG values, with the interpolation weighted by  $p$ . That is, the tendency at each point was only applied for one FMG time step. Thus, at the completion of the move, both CMG and FMG have values at appropriate points in time and space, and the integration continues.

Another possibility of defining new values after the move was also examined. This involved the use of the values at the current time level only, which were obtained as described above. A Matsuno (Euler "backward") time step was then taken in the CMG and the tendencies determined the FMG external boundaries as before. After a similar restart in the FMG, the integration continued in the normal fashion. The only disadvantage to this method may be the undesirability of frequent restarts as would be the case in a rapidly moving system. Thus, any FMG movement discussed in the remainder of this report will be the former method of interpolation.

## B. LINEAR CASE

In the previous sections, the mutually determined boundary conditions were shown to be computationally stable under





certain conditions in the linear case. Examination of the use of different time increments in each grid while moving the FMG must be numerically treated. The non-dimensional form of (1) when scaled as previously described is

$$\frac{\partial u}{\partial t'} = - \frac{\partial u}{\partial x'} \quad (5)$$

In the numerical integration of (5), centered space and time differencing is used with  $\frac{\Delta t'}{\Delta x'} \sim 1$  for each grid. An initial state, which represents a sharp perturbation, or spike, within an otherwise undisturbed field, is given by the non-dimensional expression

$$u(x', 0) = f(x') = \frac{1}{2} [1 + \cos \frac{2\pi}{L} (x' - x'_0)]$$

over one wavelength  $L$  with  $u = 0$  elsewhere. This initial state is depicted in the lower left portion of Figure 9, as well as the analytic solution at non-dimensional times  $t' = 1$  and  $t' = 2$ . Accuracy of the numerical solution may be measured by comparing the amplitude squared and phase velocity of the final numerical solution to the exact solution.

As the time and space increments decrease, the numerical solution will tend to approach the exact solution. The upper left and lower right portions of Figure 9 portray numerical solutions on uniform fine and coarse mesh grids at  $t' = 2$ , and may be compared to the exact solution. The coarse grid ( $\Delta x = .01$ ) produced an extremely distorted solution with a significant error in both phase velocity and amplitude squared. Trailing parasitic waves, or "wake," following the



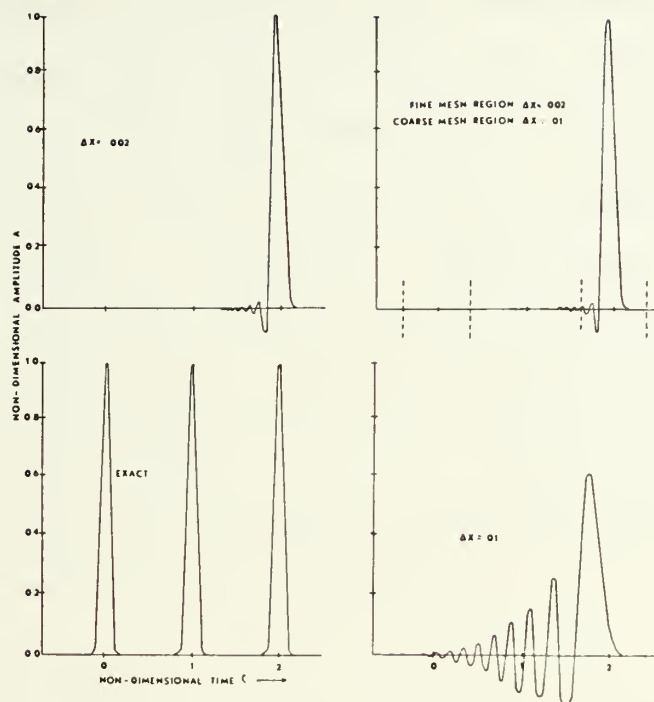


Fig. 9. One-dimensional linear case. The exact solution for  $\tau = 2$  is in the lower left panel. Numerical solutions for uniform fine grid, uniform coarse grid and meshed model are in the upper left, lower right and upper right respectively. Vertical dashed lines indicate initial and final positions of the FMG.

spike disturbance are caused by truncation error, particularly with centered space differencing (see Wurtele 1961). The numerical solution is almost equal to the exact solution when the space increment is reduced by a factor of five, as seen in Figure 9. However, the "cost" of this improved solution is the utilization of five times the computer memory and 25 times the computer time.

If the two scales are combined as previously discussed to form a meshed system, a solution very much like that in the fine mesh uniform grid is obtained as may be seen in



Figure 9. During the course of the integration, 400 time steps were taken in the CMG, while 2000 were taken in the FMG. To maintain position centered over the spike required 54 moves of the FMG toward the positive  $x$  direction. Initial and final positions of the FMG are denoted by the vertical dashed lines in Figure 9. These linear experiments demonstrate an important aspect of the meshed system, namely the analytic treatment of stability given in the previous section may be extended to the case in which different time increments are used. Moving the FMG also had no apparent deleterious effects on the solution.

### C. NONLINEAR CASE

The behavior of the meshed system in a non-linear environment is the next logical step in testing the technique. An interesting problem is the simple, but useful, example of hydraulic jump formation in a one-level hydrostatic fluid. This flow field has two characteristics which are particularly desirable for the test. First, Williams and Hori (1970) have shown that the solution is dependent on the space scale used, but in this case we can investigate the effect of reducing the grid increment only in the region of the jump. Second, the field develops sharp (eventually discontinuous) gradients in both pressure and velocity fields in a limited area.

The non-dimensional equations describing the flow in a homogeneous inviscid fluid are, in flux form



$$\frac{\partial}{\partial t} [u(\frac{1}{F} + \phi)] = -F \frac{\partial}{\partial x} [u^2(\frac{1}{F} + \phi)] - (\frac{1}{F} + \phi) \frac{\partial \phi}{\partial x} + \frac{F^2}{R_o} (\frac{1}{F} + \phi) v \quad (6)$$

$$\frac{\partial}{\partial t} [v(\frac{1}{F} + \phi)] = -F \frac{\partial}{\partial x} [uv(\frac{1}{F} + \phi)] - (\frac{1}{F} + \phi) u \quad (7)$$

$$\frac{\partial \phi}{\partial t} = -F \frac{\partial}{\partial x} [u(\frac{1}{F} + \phi)] \quad (8)$$

Following Williams and Hori (1970), the equations have been non-dimensionalized using a time scale  $T = \frac{L}{(gH)^{1/2}}$ , where  $H$  is the mean depth of the fluid, the Froude number

$F = \frac{U}{(gH)^{1/2}}$ , and the Rossby number  $R_o = \frac{U}{fL}$ . The hydraulic jump forms due to the interaction of the non-linear terms in (6) and (8), and unless the Coriolis term dominates (i.e.  $\frac{F^2}{R_o} \gg F$ ), the jump will occur at non-dimensional time of approximately  $t = 0.7$ . If the Coriolis term dominates, no jump occurs and the equations describe an inertial gravity oscillation in  $u$  and  $v$ . For this test, both the Froude number and the Rossby number were taken to be unity. Further details on an analytic treatment of the solution is given by Williams and Hori (1970), but will not be discussed further here. An appropriate non-dimensional initial state may be written

$$u(x,0) = \cos(2\pi x) \quad (9)$$

$$\phi(x,0) = F [1/8 \cos(4\pi x) + (\frac{1}{F^2} - 1/8)^2 \cos(2\pi x)] \quad (10)$$

$$v(x,0) = 0 \quad (11)$$

and is depicted in the lower left portion of Figure 10.

The numerical solutions of the energy conserving difference equations (see Williams and Hori 1970) for fine, coarse and meshed grids are portrayed in the remaining sections of





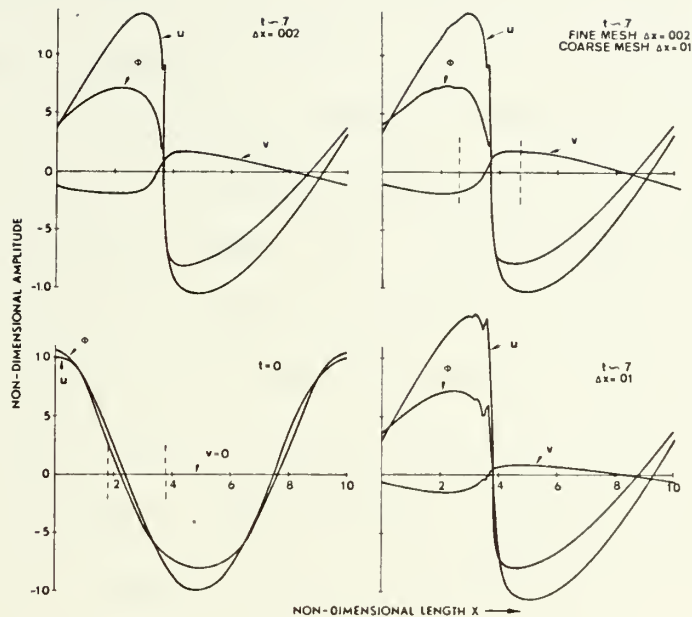


Fig. 10. One-dimensional non-linear case. Initial state (lower left), and predicted fields of  $u$ ,  $v$ , and  $\phi$  for the indicated grid scales. The vertical dashed lines represent the initial and final locations of the FMG.

Figure 10. As the gradient in the jump region increases, it becomes unresolvable in the coarse grid, and the solution quickly develops significant truncation error, resulting in a "wake" similar to that observed in the linear case. The fine grid, on the other hand, allows a superior numerical solution to be obtained, as noted in Figure 10. As in the linear case, the meshed model has virtually duplicated the solution of the uniform fine grid, although there is some noise trailing the FMG. While remaining centered over the maximum gradient in this test, the FMG moved initially nine times to the left, then 17 times to the right. The initial



and final locations are again denoted by the vertical dashed lines in Figure 10.

The one-dimensional tests of the meshing technique demonstrated several important points. First, computational stability based on the simple analytic case where the time increment was constant in both regions was demonstrated in more complex situations, where the time increment was different in each grid and the FMG was allowed to move. This is significant because use of time increments which are too small can not only reduce accuracy of the solution, but the numerical integration is much slower. Second, the movement of the FMG did not appear to have any undesirable effects on the numerical solution in either the linear or the non-linear test. Movement of the FMG will be important for many potential applications, such as following tropical storms or other embedded smaller scale synoptic systems. Third, and probably most important, the meshed model produced a forecast quite similar to that produced by a grid which is everywhere fine mesh, while requiring much less computer time and memory space. As shall be seen in the next section, this is particularly significant in a multi-level model where many dependent variables are carried, and computer memory requirements may quickly rise to machine capacity if the grid is everywhere too small. Although the uniform coarse grid utilizes even less time and memory space, the forecasts in the region of large gradients are obscured by short wavelength noise.



The one-dimensional tests also strongly indicated that the mutually determined boundary specification in the meshed model is the only scheme which is computationally stable and produces usable results, at least for centered space and time differencing. Since it is generally desirable in geophysical models to use such differencing, this is an important result. The use of an independently integrated CMG to specify FMG boundary values was shown to be unsatisfactory, even for the long wave case. Use of such a specification in a complete non-linear model would certainly lead to aliasing, and possibly to non-linear computational instability. This was also pointed out by Phillips (1972).

Another useful result of the boundary condition tests was obtained for the uniform grid. In this case, the upstream differencing at the outflow point proved to yield superior solutions even for short wavelength, high amplitude features. Although the upstream differencing boundary condition may not conserve system energy, this aspect may be unnecessary for short term forecasts. In general circulation models of the atmosphere or ocean, however, non-conservation of energy may not be acceptable. This specification should also be tested in a non-linear model to more completely determine the effect in such an environment.



## V. TWO-DIMENSIONAL, NONLINEAR EXPERIMENTS

An important step in the testing of the meshing technique is its application in a non-linear, multi-level prediction model. Since the ultimate objective of this research is the development of a meshed primitive equation model, results from a two-dimensional case will be useful for later extension to the three-dimensional system. As in the one-dimensional tests, simple analytic initial states will be imposed in the fine, coarse and meshed systems, and the forecasts from each will be compared. Boundary fluxes of heat and kinetic energy through the interface region will also be examined in both the meshed model and the corresponding portion of the fine grid model.

### A. THE PREDICTION MODEL

The primitive equations in flux form governing zonally symmetric flow in pressure coordinates are

$$\frac{\partial u}{\partial t} = - \frac{\partial vu}{\partial y} - \frac{\partial \omega u}{\partial p} + fv \quad (12)$$

$$\frac{\partial v}{\partial t} = - \frac{\partial vv}{\partial y} - \frac{\partial \omega v}{\partial p} - \frac{\partial \phi}{\partial y} - fu \quad (13)$$

$$\frac{\partial \theta}{\partial t} = - \frac{\partial v\theta}{\partial y} - \frac{\partial \omega \theta}{\partial p} + Q \quad (14)$$

$$\frac{\partial \omega}{\partial p} = - \frac{\partial v}{\partial y} \quad (15)$$

$$\frac{\partial \phi}{\partial p} = \theta c_p \frac{\partial}{\partial p} \left( \frac{p}{1000} \right)^{R/c_p} \quad (16)$$

where Q represents all sources and sinks of heat. Vertical





velocity in pressure coordinates ( $\omega$ ) is carried at 100 mb intervals between 100 and 1000 mb in the ten-level model, while the remaining variables are carried at intermediate levels as depicted in Figure 11. Potential temperature and

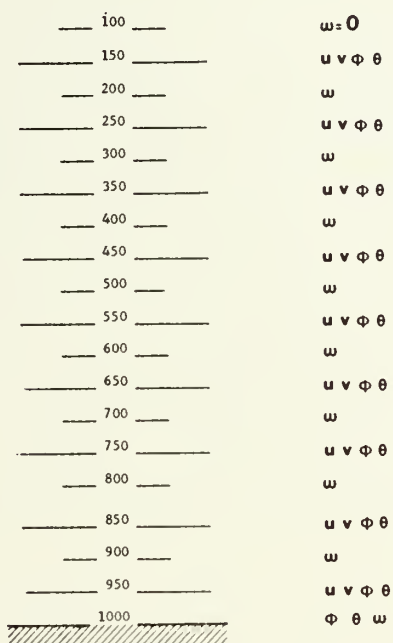


Fig. 11. Vertical distribution of dependent variables and pressure levels for the two-dimensional model.

geopotential heights are also computed at 1000 mb for use in the hydrostatic and thermodynamic equations. The north-south boundaries are insulated free slip walls, while the lower boundary condition is

$$\frac{d\phi_{1000}}{dt} = 0 \quad (17)$$

Vertical velocity is obtained by integrating (14) downward from 100 mb where  $w$  is assumed to be zero. The time integration is centered after an initial forward time step, with



certain differences in the meshed system which will be discussed later. Other aspects of the basic numerical model are given by Elsberry and Harrison (1971) and will not be discussed further here.

## B. TWO-DIMENSIONAL TESTS

An initial state representing a zonal trade wind regime of low-level easterlies replaced by westerlies aloft was achieved by imposing an appropriate horizontal temperature gradient. This initially undisturbed pattern, depicted in the vertical cross section in Figure 12, is distorted as a constant, analytic heating distribution is applied, within a relatively narrow band. The heating function was similar to that used by Holton (1971) in diagnostic experiments,

$$Q = Q_o \exp\left[-\left(\frac{y-y_o}{\alpha}\right)^2\right] \cdot \begin{cases} \frac{p_o-p}{p_o-p_{\max}} - \exp\left[-\left(\frac{p}{p-p_{\max}}\right)\right] & p < p_{\max} \\ 1 - \frac{p_{\max}-p}{\beta} & p > p_{\max} \end{cases} \quad (18)$$

Here  $p_{\max}$  and  $y_o$  are the locations in the vertical and horizontal where the heating function is a maximum. The parameter  $\alpha$  determines the relative latitudinal extent of the heating pattern and  $\beta$  determines the rate at which the function decreases above the maximum vertical level. The vertical section of the heating plotted in Figure 12 results when the following parameters are chosen

$$\begin{aligned} Q_o &= 5 \times 10^{-5} \text{ deg sec}^{-1} \\ \alpha &= 1.0 & \beta &= 200 \text{ mb} & p_{\max} &= 500 \text{ mb} \\ p_o &= 1000 \text{ mb} \end{aligned}$$



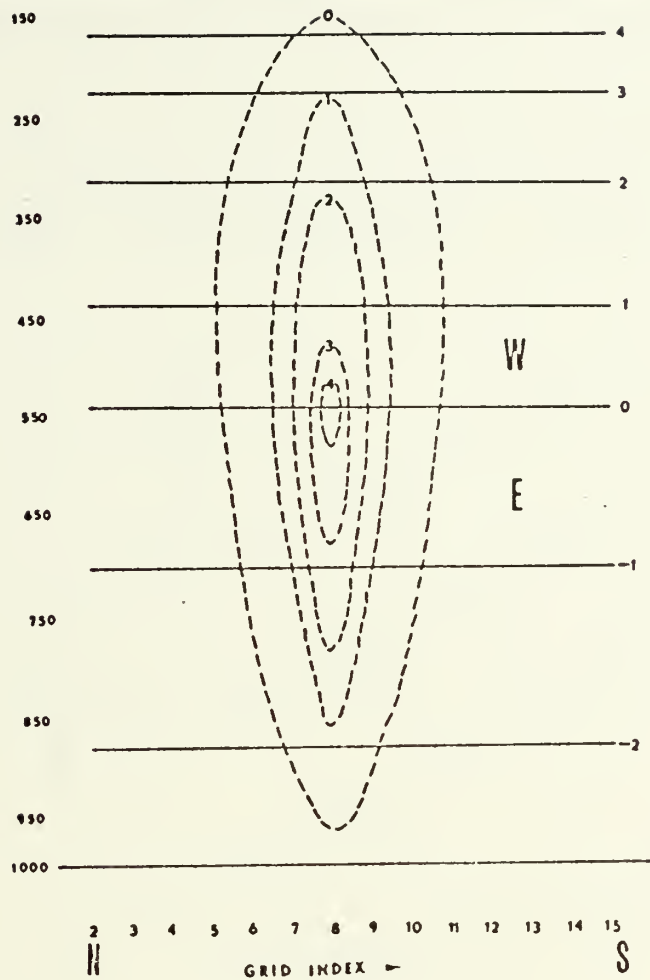


Fig. 12. Initial wind field (solid) in  $\text{ms}^{-1}$  vs pressure. The heating pattern (dashed) is a maximum at 550 mb, with isolines labeled in  $\text{K day}^{-1}$ .

This heating pattern simulates the heat released by a zonally symmetric band of convective elements. To offset this heating, radiative cooling over the region was chosen such that the net heating at each pressure level was zero. In the coarse grid, most of this heating will be applied at the point  $y = y_0$  (see Figure 12), while in the fine grid with one-fifth the space increment, the heating will be smoothly applied over many grid points. The sum ( $Q$ ) of the imposed



heating and compensatory radiational cooling in (14) is chosen so that the volume integral of heat energy is constant in time.

Figure 13 depicts the 24 hour forecast field of 1000 mb heights for each of the three models. For this forecast,

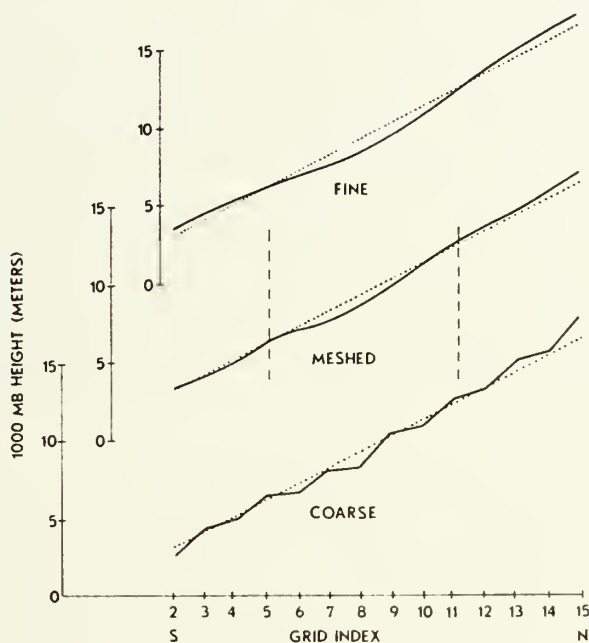


Fig. 13. Predicted heights at 1000 mb (solid) for the models indicated. 480 time steps have been taken in the CMG and uniform coarse grid, while 2400 have been taken in the FMG and uniform fine grid.

480 three minute time steps were taken in the coarse mesh region ( $\Delta X = 45\text{nm}$ ), while 2400 time steps were required in the fine mesh regions of the uniform and meshed models, because of the factor of five in the spatial increment. The effect of the localized heat source in the uniform coarse grid is quite evident as can be seen in the lower portion





of Figure 13. Because nearly all the thermal forcing is applied at one grid point (column) in the coarse grid, a  $2\Delta x$  mode is excited. The corresponding forecasts by the meshed and fine grid models are shown in the center and upper portion of Figure 13 respectively. In the area of maximum heat release of both systems, nearly identical 1000 mb height fields are predicted. Even in the CMG of the meshed model, the forecast is quite similar to that plotted for every fifth point within the uniform fine grid system. Perhaps a more sensitive indicator of the performance of the meshed model is the response of the vertical motion field to the imposed heating pattern. Figure 14 depicts this field

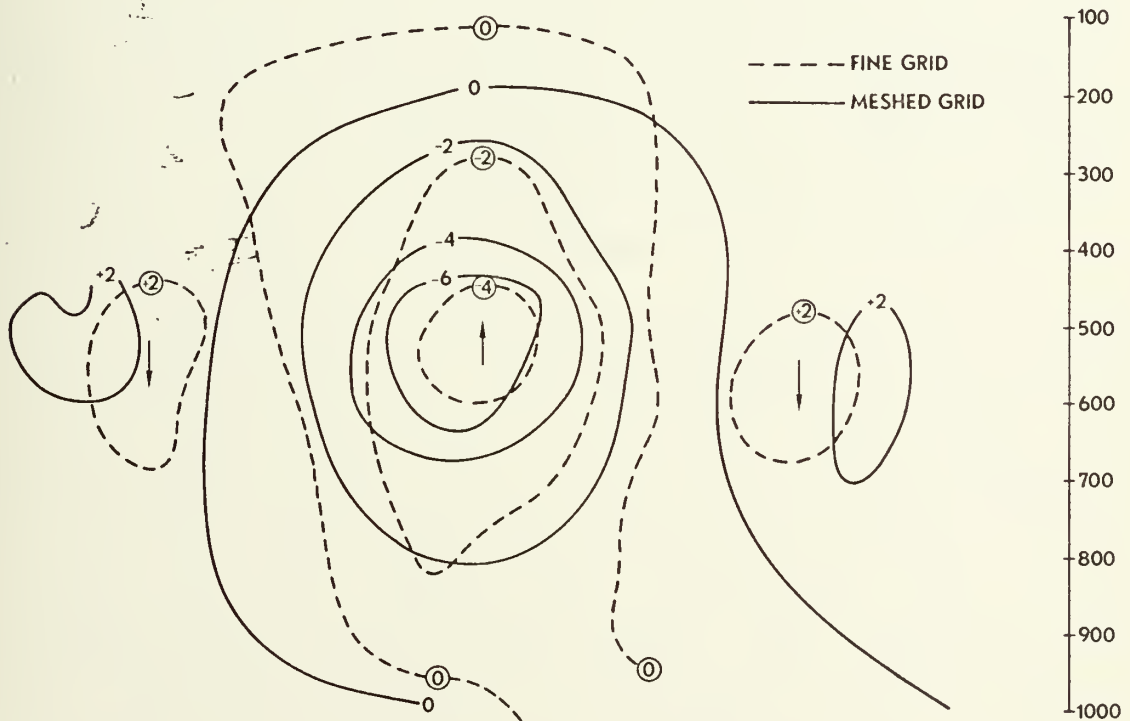


Fig. 14. Vertical section of the 24 hour vertical motion in  $\text{mb sec}^{-1} \times 10^4$  for the FMG (solid) portion of the meshed model, and the corresponding region of the uniform fine grid model (dashed).



for the meshed and uniform fine grid within the FMG region of the meshed model. Very little vertical motion occurs outside this limited area and is therefore not portrayed. A deep region of ascent is produced by the heating, with weaker compensating descent on either side. In the meshed grid, the ascent cell was stronger and slightly wider after 2400 FMG time steps, probably due to non-linear effects at the interface. The heat gains within the FMG meshed region must be transferred horizontally because of the requirement for heat balance at each level, and boundary fluxes across the interface are an important consideration.

The accumulated boundary fluxes of kinetic and thermal energy through the interface in the meshed system, and the corresponding area in the uniform fine grid, may be obtained by integrating these fluxes in the vertical and around the entire area after each FMG time step. In Table 2, this comparison is made for kinetic energy between the two grid systems. The row labeled "inner" refers to the FMG portion of the meshed model, and the corresponding area of the uniform fine grid system, with the remainder of the grid area represented by the "outer" row of data. The larger generation in the meshed system is due to the somewhat stronger ascent cell, but despite this, the boundary flux of kinetic energy was the same in both models. The dissipation quantity for the meshed model is a result of a horizontal momentum diffusion term used in this system and will be discussed later. No dissipative terms are included in the other



Table 2. Kinetic energy balance for meshed and uniform fine grid models (joules  $\text{cm}^{-2} \text{ day}^{-1}$ ).

	$\Delta$ KE	Generation	Dissipation	Boundary Flux	
Fine Grid	Inner	+2.08	+2.54	0	-0.46
	Outer	+1.51	+1.05	0	+0.46
Meshed Grid	Inner	+2.38	+3.77	-0.93	-0.46
	Outer	+1.25	+0.79	0	+0.46

formulations, thus the balance is mainly between boundary flux and generation. The qualitative comparison of the kinetic energy balance is good, with the total kinetic energy change over the entire forecast region almost identical in both systems.

Because the radiational cooling exactly offsets the imposed heating, the net change in thermal energy in Table 3 is necessarily zero over the entire forecast region. The slightly larger boundary flux of thermal energy in the meshed system is again due to slight inconsistencies at the interface. As in the case of the kinetic energy balance, the qualitative comparison of the models in Table 3 is excellent, with less than three percent difference in the boundary fluxes.



Table 3. Thermal balance for meshed and uniform fine grid models ( $\text{deg.pot.temp.cm}^{-2}\text{day}^{-1}$ ).

	$\Delta\theta$	Heating	Cooling	Boundary Flux	
Fine Grid	Inner	+4.93	+188.98	-78.21	-105.84
	Outer	-4.93	0	-110.77	+105.84
Meshed Model	Inner	+2.48	+188.98	-78.21	-108.29
	Outer	-2.48	0	-110.77	+108.29

#### C. COMPUTATIONAL DEVICES USED IN THE MULTI-LEVEL MODEL

Early tests not discussed in this paper were conducted to examine the behavior of the meshing technique in the primitive equation model. In these tests, two aspects related to the interface boundary conditions and the centered space and time differencing became evident. Spatial separation in the FMG resulting from slight inconsistencies in the imposed boundary condition created the first problem. Although the solution on the FMG near the interior coincident point is "nearly exact," the CMG solution at the external interface is not as accurate, and will differ somewhat from one obtained on a uniform fine grid, even though the integrations are simultaneous. The tacit assumption of





linearity over each CMG time step also adds to the inconsistency. Once spatial separation existed within the FMG, setting the CMG boundary values over an odd number of steps triggered high speed internal gravity waves which propagated from the interface into the CMG. When reflected from the north-south walls, the gravity waves tended to interact with those propagating in the opposite direction and growth on a small scale was observed, eventually leading to non-linear computational instability. The minor spatial variations at the interface were eliminated by applying an area (line) average of the surrounding five points, rather than the point value at the single coincident point. As a final constraint on the spatial separation in other regions of the FMG, a horizontal momentum diffusion term of the Laplacian type was employed in this portion of the model. A relatively small coefficient of  $10^4 \text{ m}^2 \text{ s}^{-1}$  was sufficient to control the separation.

Even with the spatial separation controls discussed above, the slight inconsistencies in the boundary values derived from the CMG solution caused the solution in the FMG to begin to separate in time. This was a small effect, but after several hundred steps in the FMG, it was evident that a control was needed. Thus, Matsuno (Euler "backward") restarts at experimentally determined intervals were periodically applied in the FMG and the time separation was eliminated. These controls on the meshed system appear to have very little effect on the accuracy of the solution as



evidenced in the last section. While it is true that higher order differencing and/or interpolation schemes might eliminate the need for these simple controls, the additional computation time required for such formulations would probably negate their value. Even with the centered space and time differencing, the time increase for the integration in a three-dimensional meshed model will not be trivial.

It is clear from examination of Tables 2 and 3 that the meshing technique conserves total thermal and kinetic energy when the finite difference equations are written similarly to the energy conserving flux form described by Arakawa (1966). This is important not only because of computational stability criteria, but also for long term application. General circulation models of the atmosphere and ocean often require increased resolution in certain areas, and it is crucial that no spurious sources or sinks of energy are introduced by modifications to the grid network.



## VI. THREE-DIMENSIONAL EXPERIMENTS WITH A PRIMITIVE EQUATION MODEL

The one- and two-dimensional tests demonstrated the computational stability of the meshing technique in a variety of environments. Nonlinear two-dimensional cases illustrated that realistic energy exchanges occurred at the interface, and that improved solutions were obtained with the meshed grid system. The three-dimensional cases discussed below will demonstrate that these features of the meshing technique are maintained in more complex situations.

Important aspects of three-dimensional meshed grids are initialization of the fine mesh region, physical size of the fine mesh region and ratio of grid increment reduction. The latter two considerations are strongly interdependent for three-dimensional models, since from computer memory and time viewpoint, increasing the physical size of the FMG restricts the grid scale reduction. On the other hand, the FMG must be large enough to completely encompass the region of interest, but still have a ratio of reduction to a small enough spatial increment so that the FMG can allow development on the scale desired. Thus, one must evaluate the type and scale of the feature of interest, and design the FMG with these in mind. For example, the same FMG specifically designed for tropical storm studies would probably be unsuitable for a frontal scale feature. In the latter case, an



FMG with larger physical size, but with a smaller scale reduction would be more appropriate.

An extension of the concept of optimizing FMG design to suit the scale of the feature of interest is to utilize a gradual reduction in grid scale. This would essentially allow one to "focus" on a region of interest with a very fine grid, while still maintaining relatively fine resolution in the surrounding area. Certain difficulties and limitations associated with this type of model arise from application of the mutually determined boundary specification, and will be discussed in detail in a later section. A primary advantage of the gradual reduction model is the reduction of computer memory and time required to obtain improved solutions over the same area as an abrupt reduction to the smallest scale.

As in the earlier tests, simple analytic initial states were used in the three-dimensional models to idealize the initial conditions. This idealization is desirable since the primary objective of these cases was to demonstrate the meshing technique in the single reduction (SR) and multiple reduction (MR) models, observe the effect on the large scale solution, and compare the results to those obtained on a uniform coarse grid. Improvements to all the versions of the model would have to be accomplished through real data forecasts, with subsequent statistical verification. There are, for example, many possible ways to initialize the FMG, and many real data tests would need to be made to determine





the optimum method. Other facets of the meshed models, such as diffusion coefficient magnitude, frequency of restarts, etc., have only been cursorily examined in this report and could probably be optimized through further numerical testing.

#### A. THE PREDICTION MODEL

The basic model utilized in all three-dimensional experiments was similar to that described by Harrison (1969) and Elsberry and Harrison (1971, 1972), except that fewer levels in the vertical were used. As in the two dimensional case, the equations written in flux form are

$$\frac{\partial u}{\partial t} = -L(u) + fv - m \frac{\partial \phi}{\partial x} \quad (19)$$

$$\frac{\partial v}{\partial t} = -L(v) - fu - m \frac{\partial \phi}{\partial y} \quad (20)$$

$$\frac{\partial \theta}{\partial t} = -L(\theta) + Q \quad (21)$$

$$\frac{\partial \omega}{\partial p} = -m^2 \left[ \frac{\partial}{\partial x} \left( \frac{u}{m} \right) + \frac{\partial}{\partial y} \left( \frac{v}{m} \right) \right] \quad (22)$$

$$\frac{\partial \phi}{\partial p} = \theta c_p \frac{\partial}{\partial p} \left( \frac{p}{1000} \right)^{R/c_p} \quad (23)$$

where  $Q$  represents all sources and sinks of heat and

$$L(S) = m^2 \left[ \frac{\partial}{\partial x} \left( \frac{Su}{m} \right) + \frac{\partial}{\partial y} \left( \frac{Sv}{m} \right) \right] + \frac{\partial}{\partial p} (\omega S)$$

for a general variable  $S$ . The map factor is  $m$ , with the grid on a Mercator projection true at 22.5N. The vertical distribution of variables and pressure levels in the three-dimensional version is depicted in Figure 15, with the upper and lower boundary conditions identical to those in the two-dimensional model. The north-south boundaries of the three-



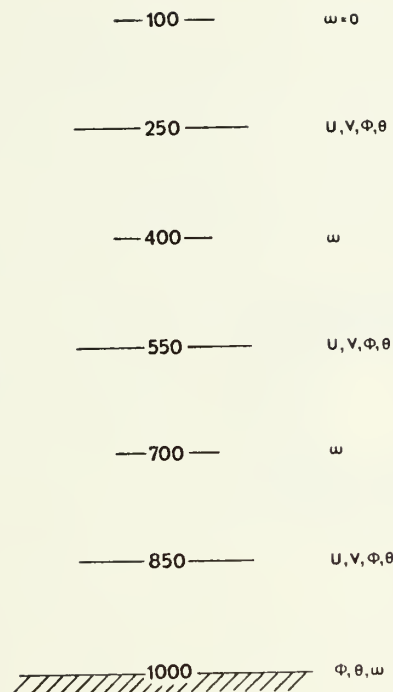


Fig. 15. Vertical distribution of dependent variables and pressure levels for the three-dimensional models.

dimensional model are insulated, free-slip walls, while cyclic continuity is assumed in the east-west direction. As in the two-dimensional case, the difference equations were written similarly to the energy conserving form described by Arakawa (1966).

An example of a horizontal grid level for the SR meshed system is depicted in Figure 16. The CMG indices shown are acronyms by which the location of the FMG may be determined. For example, IWE represents index I(east-west), West side, and External interface. Thus, if IWE and JSE are known, the location of the FMG is uniquely determined, and these, of course, are time dependent as the FMG moves. To avoid



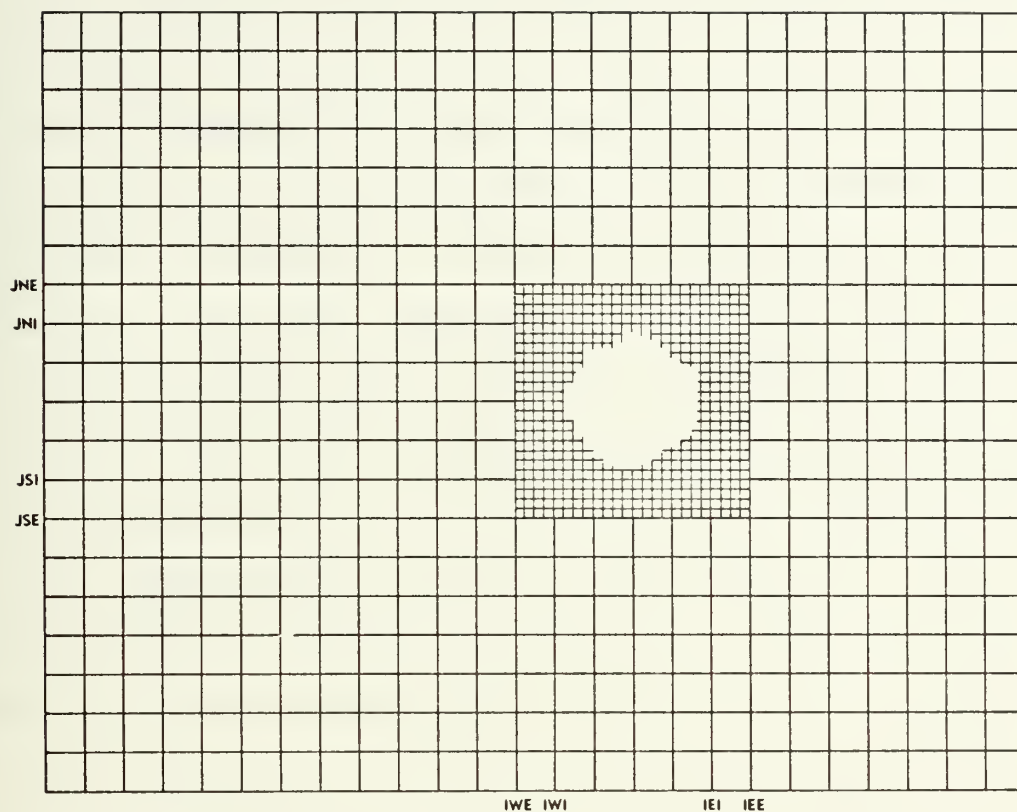


Fig. 16. An example of a horizontal pressure level for the three-dimensional meshed model. For the example shown, the FMG increment is one-fourth that of the CMG ( $p = 4$ ), and the FMG covers six CMG intervals in each horizontal direction.

interaction with the CMG boundaries, the FMG is not allowed to move within three CMG grid intervals of the walls, or the east-west extremes of the grid. For these tests, the CMG spatial increment was 180 nm, and for the SR model, the FMG increment was 36 nm ( $p = 5$ ). Because of excessive computer memory and time requirements, no uniform fine grid comparisons were possible for any of the three-dimensional experiments. Other than the restrictions above, the location of the FMG shown in Figure 16 is quite arbitrary. Details



of the MR model will not be discussed in this section, and the first series of tests to be described utilized the SR model with  $p = 5$ .

The CMG used for all three-dimensional tests was  $25 \times 20$  in the east-west and north-south directions respectively, as may be seen in Figure 16. In the SR meshed model, the FMG covered  $6 \times 6$  CMG grid intervals, or a  $31 \times 31$  FMG. Because  $p = 5$  in this model, the time step in the FMG was one-fifth that in the CMG, and it is quite evident that the FMG calculations required most of the computer time, since the number of total calculations increases as the cube of  $p$ . This again indicated the desirability of keeping the FMG just large enough to encompass the region of interest. It was experimentally determined that each time step took approximately eight times longer in the meshed system, as opposed to the uniform coarse grid. This may be compared to the time increase of about 125 times for a uniform fine grid over the entire region of the coarse grid model.

Initial location of the FMG is achieved by identifying the desired location and appropriately defining IWE and JSE (see Figure 16). At the interior coincident points (ISI, JSI, for example) the CMG boundary values were determined by an area average of the surrounding 25 FMG values before each CMG time step. For convenience in the actual coding, all the interior coincident points were replaced by the area average, realizing that no forecasts are made at the CMG points which lie within the FMG area. After each complete





time step in the CMG, the tendencies around the external interface were spatially and temporally interpolated. As in the earlier experiments, the FMG external boundaries were then updated after each FMG time step. Movement of the FMG was accomplished in exactly the same manner as in the simpler models.

## B. INITIALIZATION OF THE MESHED GRID SYSTEM

Initialization of the FMG is an important point to consider in the meshed model. Since mesoscale data are seldom available, there are two basic alternatives, that is to either attempt a fine grid analysis or to interpolate data from the CMG. Hill (1967) has compared fine grid analysis to interpolation for initialization of the FMG, and noted that if analyzed data are used, the effects of errors in height or temperature gradients increases as the grid distance decreases. It would seem logical, therefore, that interpolation from the CMG is the only real alternative, unless perhaps an objective analysis scheme was used, with basically the same order interpolation as the interpolation from the CMG. If mesoscale data are available, however, one might consider modifying the interpolated values. For example, if the interpolated data were to undergo a diagnostic phase such as the balance equation, the observed mesoscale data could be incorporated before the diagnostic phase, thereby enhancing the representativeness of the analysis. Since no small (sub-grid) scale data can be added by interpolation, one must hope that the elements of the small scale



will naturally develop during the integration as a result of the large scale forcing or parameterized fluxes of heat, moisture and momentum (e.g. Bushby and Timpson 1967). This is a fundamentally crucial concept to fine mesh forecasting, for if it is not true, grid increments need be no finer than the distance between observation stations.

After the FMG data has been interpolated from the CMG, several alternatives exist. That is, the values of the dependent variables may be used as is, or undergo some type of diagnostic phase. Wang and Halpern (1970) have compared the use of pure interpolated data versus that which had been balanced by means of the linear balance equation, and obtained better results with the interpolated data. Their model was barotropic, and smoothers were used, so it is difficult to evaluate their results as applied to the multi-level primitive equation model. Thus several experiments were conducted to evaluate the optimum initialization for the analytic initial states. The first attempt was to merely derive all values of the dependent variables from the CMG to the FMG by linear interpolation, and start the integration with no diagnostic phase. Almost immediately, large amplitude very short wavelength gravity waves were excited, and aliasing very quickly led to non-linear computational instability. Pure interpolation was clearly unsatisfactory for the meshed model, at least when only small diffusion was employed, and there was no implicit mechanism for selectively damping high frequency modes.



A consistent diagnostic equation which uses winds to derive heights may be obtained by forming a divergence equation from (19) and (20). Such an equation is particularly applicable where the Rossby number  $U/fL$  is not small, such as in the tropics, or for small scale disturbances. The equation may be written

$$\begin{aligned} \frac{\partial}{\partial t} \left( \frac{\partial u}{\partial x} + \frac{\partial v}{\partial y} \right) = & - \frac{\partial}{\partial x} L(u) - \frac{\partial}{\partial y} L(v) + f \left( \frac{\partial v}{\partial x} - \frac{\partial u}{\partial y} \right) \\ & - u \frac{\partial f}{\partial y} - \frac{\partial m}{\partial y} \frac{\partial \theta}{\partial y} - m \nabla^2 \phi \end{aligned} \quad (24)$$

This divergence equation as shown is not exactly consistent with the form of the continuity equation (22), but because the map factor was taken to be unity for these experiments, the additional multiplications by  $m$  are not shown. In the first SR model test to be described (tropical storm simulation), the winds at all levels were analytically imposed. The divergence equation (24) was then solved by sequential overrelaxation to obtain the geopotential heights, and hence temperature, with the assumption that the time change in divergence is zero over one time step. For this case, the original winds were non-divergent, but it should be noted that this is not necessary for real data or interpolated data. In the second SR test (frontal simulation), the FMG was initialized quite differently. In this case, data were obtained from a forecast on the uniform coarse grid model. This data was thus the result of several model days of integration, and hence the vertical motion fields were well developed. Winds were interpolated from the CMG to the FMG,



and a consistent vertical motion field was obtained from (22) and so the nonlinear terms in (24) were complete. This approach was the last one tested during this research, but seems to show promise as a possible technique when real data is used to initialize the model. In all SR and MR experiments, the CMG was initialized with the use of (24), and boundary conditions for this grid are those suggested by Elsberry and Harrison (1971) and will not be discussed here.

#### C. SR TEST 1: A SIMULATED TROPICAL STORM WITH DIABATIC HEATING

An important meteorological application of nested grid systems is in tropical prediction models. Formation, development and subsequent movement of tropical storms and similar disturbances could be more accurately predicted by a properly located FMG. The first three-dimensional test to be discussed involved the SR model, and an analytic simulation of a tropical storm scale disturbance. As noted earlier, analytic initial states were used throughout in order to idealize the initial conditions for the tests of the meshing techniques. Forecasts of the movement and development of the simulated disturbance were then compared for the meshed and uniform coarse grid models. Boundary fluxes, kinetic energy balance and temperature patterns are treated in detail in this test, as well as several other aspects of the integration.

The storm simulation was kept as simple as possible to isolate possible effects of the meshed system on the





numerical solution. An isolated low pressure center in the trough of a wave in the easterlies may be simulated by specifying the winds uniformly at all levels by

$$u = - \frac{1}{f_0} \frac{\partial \phi_0}{\partial y} \quad (25a)$$

$$v = \frac{1}{f_0} \frac{\partial \phi_0}{\partial x} \quad (25b)$$

where

$$\phi_0 = F(y) + H_2 \sin(k_1 x) \sin(k_2 y) - H_2 \exp\left(\frac{x-x_0}{\alpha}\right) \exp\left(\frac{y-y_0}{\beta}\right) \quad (25c)$$

Since the winds are constant in the vertical, the initial disturbance is a circularly symmetric, non-divergent vortex. The expression for  $\phi_0$  is convenient, because the size, shape and location of the resulting balanced low center are easily controlled. The independent variables in (25) have been normalized by the length and width of the domain for simplicity. The magnitude of the basic zonal flow was approximately  $4.5 \text{ m s}^{-1}$ , and is determined by  $F(y)$ , a linear function of latitude. The amplitude of the wave in the easterly flow is governed by  $H_2$ , while the central value of  $\phi_0$  is determined by  $H_3$ . The parameters  $\alpha$  and  $\beta$  govern the longitudinal and latitudinal extent of the depression center, and  $k_1$  and  $k_2$  are the domain wavelengths in the east-west and north-south directions respectively. The low center may be appropriately located in the trough by specifying  $x_0$  and  $y_0$  to coincide with the minimum values determined by the middle term in (25c).



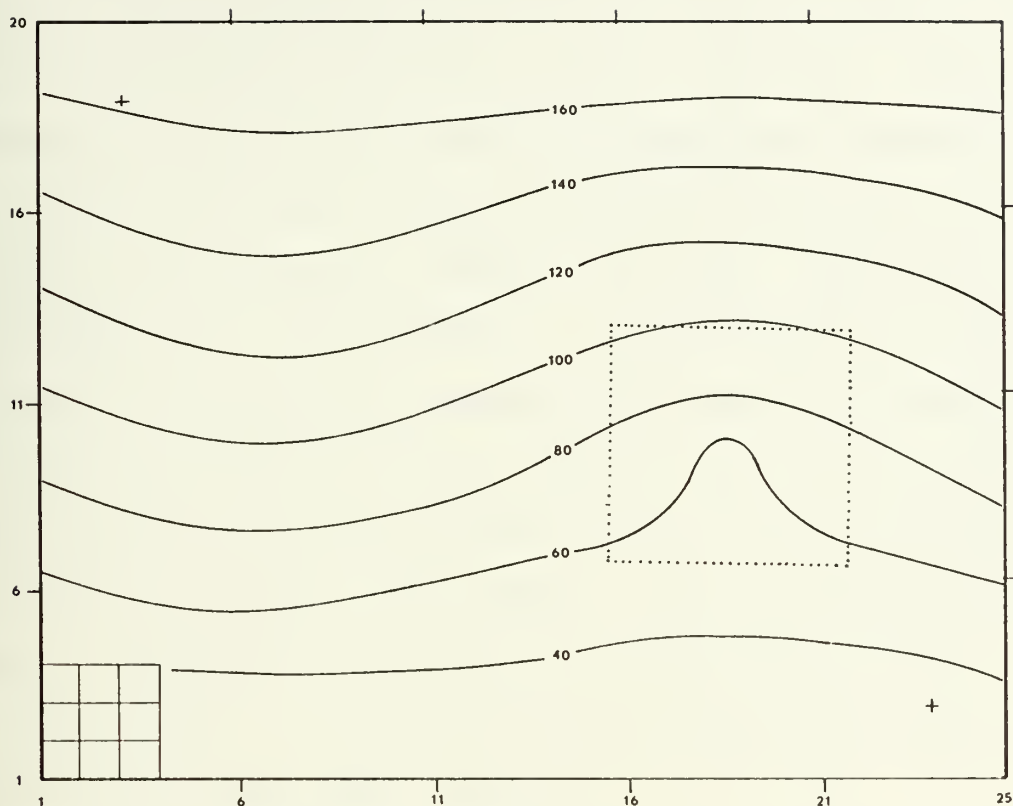


Fig. 17. Balanced height field (m) -1400m at 850 mb after initialization procedure described in text. The initial location of the FMG is denoted by the dotted outline. The CMG and uniform coarse mesh grid scale is indicated in the lower left corner.

Figure 17 depicts the resulting balanced height pattern in the CMG for the following choice of parameters:

$$H_2 = 150 \text{ m}^2 \text{ s}^{-2}$$

$$H_3 = 200 \text{ m}^2 \text{ s}^{-2}$$

$$\alpha = 1$$

$$\beta = 1$$

$$k_1 = 1$$

$$k_2 = .5$$



After the CMG balanced geopotential heights were obtained, each of these parameters, as well as  $L(u)$  and  $L(v)$  in (24) were interpolated around the external interface. These values were held fixed during the subsequent diagnostic phase of the FMG, and thus assured a consistent merging of the two scales in the interface region of the FMG. Specifying the geostrophic wind analytically in the FMG creates a simulation of enhanced data in this region. The values at interior coincident CMG grid points were exactly those which would have been obtained by interpolation, but there was no assumption of linearity between these points. In an extremely idealized sense, this had the same effect as subjective modification of the initially interpolated FMG data with mesoscale data obtained from some other source.

That portion of the 850 mb geopotential height field within the dotted outline of the FMG in Figure 17, may be compared with Figure 18, which depicts the same field resulting in the FMG when the above initialization is carried out. Near the interface there is a smooth blend, because of the boundary conditions discussed in the preceding paragraph. In the interior of the FMG, however, there is more detail in the initial state. Addition of such data would clearly improve the forecast in the FMG, and perhaps simulate development of features on this scale.

#### 1. Heating for the Tropical Storm Simulation (SR Model)

Development of the simulated storm was artificially induced in a manner similar to that used in the two-



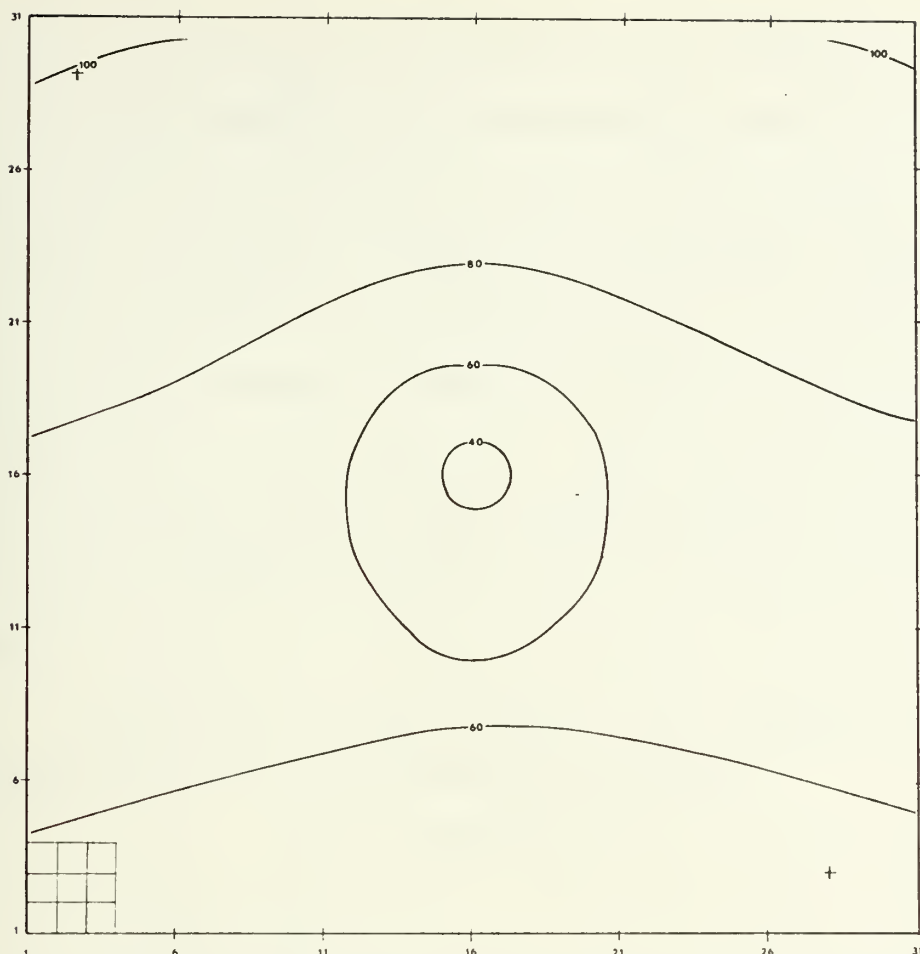


Fig. 18. Balanced height field (m) -1400m at 850 mb in the FMG following the initialization described in the text. The FMG grid scale is indicated in the lower left corner.

dimensional test. In actual tropical storms, one expects to find maximum latent heat release in approximately the middle portion of the troposphere, thus an analytic heating function was used to simulate such heating. This function had the advantage that it could easily be positioned in both the vertical and horizontal and is given by

$$Q = Q_o \exp \left[ - \left( \frac{x-x_o}{\alpha} \right)^2 \right] \exp \left[ - \left( \frac{y-y_o}{\beta} \right)^2 \right] \cdot \quad (26)$$

$$\left\{ \begin{array}{ll} \frac{p_o - p}{p_o - p_{\max}} - \exp \left[ - \left( \frac{p}{p - p_{\max}} \right) \right] & p < p_{\max} \\ 1 & p = p_{\max} \end{array} \right.$$





where  $x_0$ ,  $y_0$  and  $p_{\max}$  are the horizontal and vertical locations of the heating maximum. The parameters  $\alpha$  and  $\beta$  determine the longitudinal and latitudinal extent of the heating. The relative lack of vertical resolution in the model caused more than half of the heating to be applied at  $p_{\max}$ . To simulate heating at levels between 550 mb and 250 mb, the heating at 250 mb was set equal to that at 850 mb. As in the two-dimensional case, a radiation profile was derived such that the net heating at each pressure level was zero for the entire spatial domain.

The heating pattern for the FMG at  $p_{\max}$  is depicted in Figure 19 for the following parameters:

$$\begin{aligned} Q_0 &= 5 \times 10^{-5} \text{ K s}^{-1} \\ \alpha &= 1 \\ \beta &= 1 \\ p_{\max} &= 550 \text{ mb} \\ p_0 &= 1000 \text{ mb} \end{aligned}$$

The heating distribution in the uniform coarse grid (not shown) was slightly different because the area averages of the FMG heating were applied at coincident points, but the net heating over the entire spatial domain was the same for both models. In both uniform coarse grid and SR models, the horizontal heating maximum was linked to the location of the 1000 mb low center. In the FMG of the SR model, the location shifted with the 1000 mb low center in intervals of one FMG spatial increment. Thus in the FMG, the heat source was always in approximately the proper location to enhance



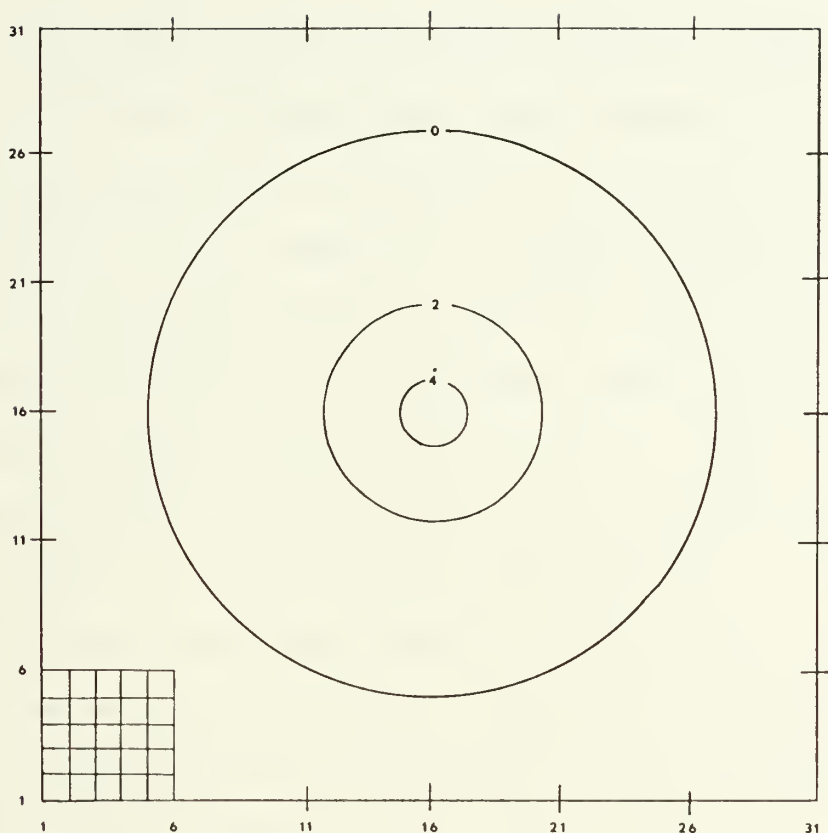


Fig. 19. Heating distribution ( $\text{K day}^{-1}$ ) in the FMG at  $p_{\text{max}}$  (550 mb). The distribution at the other levels was similar, but with smaller values. The FMG grid scale is indicated in the lower left corner.

the generation of kinetic energy. In this manner, the link between boundary layer ascent and latent heat release (conditional instability of the second kind, or "CISK") was roughly simulated. When the FMG moved (one CMG increment), the heating maximum was redefined over the new location of the low center in the FMG. This small scale detail was, of course, not possible in the uniform grid model, where the



heating maximum location was shifted in increments of one CMG spatial interval, again dependent on the 1000 mb low center.

It is apparent that proper location of heating with respect to the depression center will improve the forecasts of both development and movement, at least in a fine grid. This may not be true, however, in uniform coarse grid models. Elsberry and Harrison (1972) showed that the use of different parametric latent heating schemes had little effect on the predicted movement of hurricane Betsy (1965) in a uniform coarse grid, ten-level primitive equation model. Although Elsberry and Harrison's model was very complete in that friction, latent and sensible heating and radiation were included, the movement can only be subjectively determined by "guessing" at the location of the low center at the completion of the forecast. Thus as the grid scale decreases, the location may be more accurately determined, thereby yielding a more valuable movement forecast. Also, as the scale decreases, the parametric relationships probably become more valid, since the underlying assumptions have greater physical meaning on a smaller scale. It seems reasonable to expect higher verification score in real data cases, when the same parametric schemes are employed in the meshed system, as opposed to a uniform coarse grid model such as that used by Elsberry and Harrison (1972).



## 2. Results of the SR Tropical Storm Simulation Case

Two significant results of the tropical storm simulation in the SR model involved the movement and development of the low center. The phase error of short wave systems is strongly linked to the finite grid scale, and, as seen in earlier linear experiments, the meshed model reduces the error. Reduction of phase error is particularly crucial in predicting the movement of tropical storms, where accuracy is extremely important.

The predicted 48 hour, 850 mb height field for the uniform coarse grid is depicted in the upper portion of Figure 20, with the same forecast for the meshed model shown in the lower panel. The meshed model result was obtained by analyzing the CMG prediction, but replacing interior coincident values by those from the FMG forecast. Since the actual forecast location of the low center in the FMG was between CMG grid points, this location was, therefore, taken from the FMG forecast. As may be seen in Figure 20, the meshed model predicts greater westward movement of the low center than the uniform coarse grid model. Since the mean zonal flow velocity was approximately  $4.5 \text{ m s}^{-1}$ , a pure advective westward movement of about 775 km would be expected during the 48 hour forecast. Location of the low center in the uniform coarse grid is rather subjective, and thus movement is difficult to ascertain with accuracy finer than the grid scale itself, but Table 4 summarizes the two main





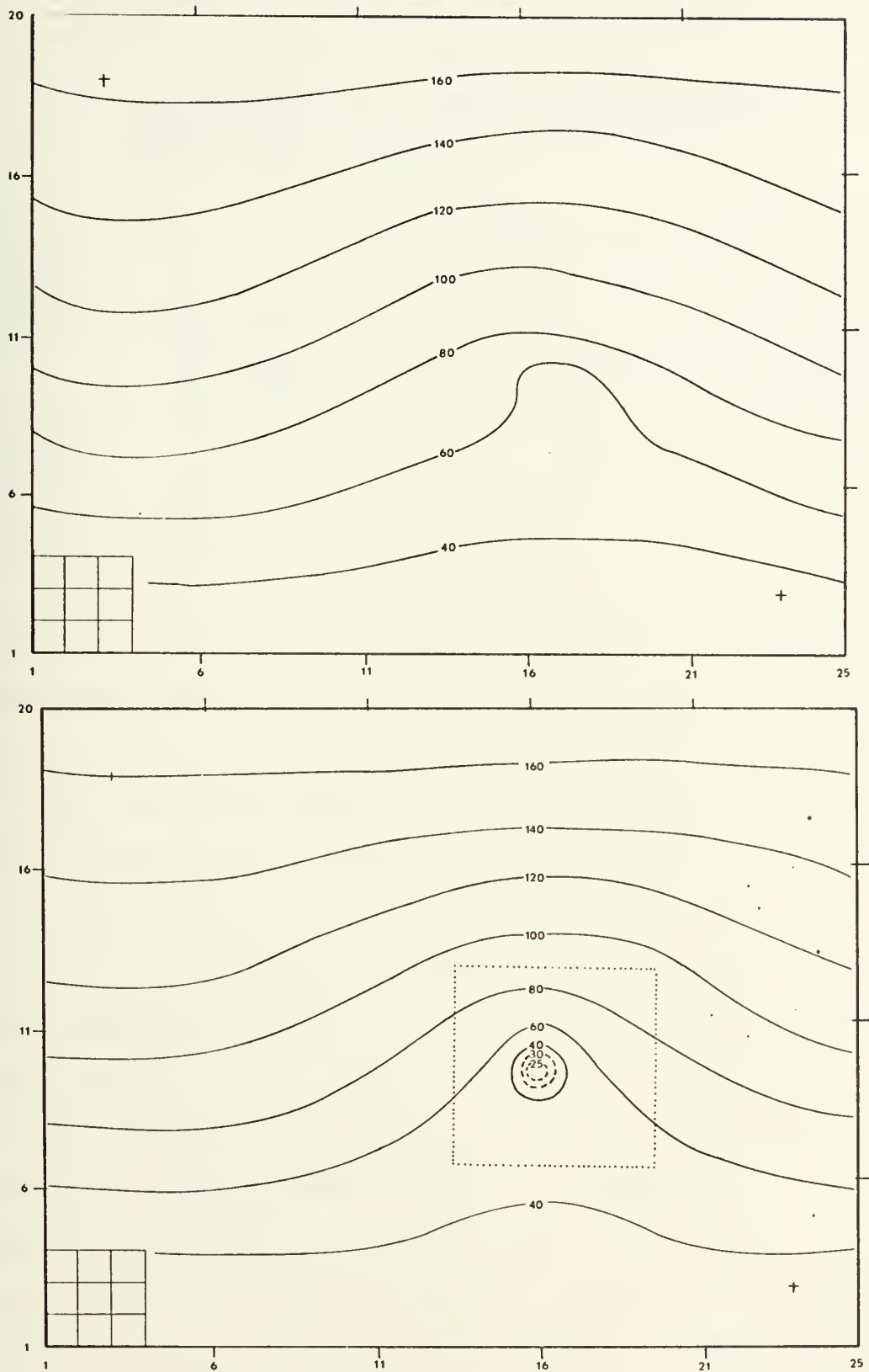


Fig. 20. Prediction of 850mb heights (m)-1400m at 48 hours. The upper portion is the uniform coarse grid forecast, the lower that of the meshed model. See text for details.



Table 4

Comparison of the uniform coarse grid and meshed model 48 hr height forecasts at 850 mb (low center)

Model	Movement		Development		
	Distance (km)	Direction	Initial (m)	Forecast (m)	Change (m)
Uniform coarse	600	W	1457	1454	-3
Meshed	720	W	1437	1422	-15

facets of the prediction, that is movement and development. The meshed model presented distinct advantages in evaluating the forecast fields of the dependent variables. An example of the detail available is portrayed in Figure 21, the 48 hour forecast 850 mb heights. Location of the low center was accurate to the scale of the FMG, thus both location and direction of movement were more accurate. This information was then transferred to the large scale analysis shown in the lower portion of Figure 20, which is perhaps more convenient for display purposes. Thus the additional detail available from the FMG forecast is incorporated into a large area analysis in a consistent manner. The initial and final positions of the FMG are denoted by the dotted outlines in Figure 17 and Figure 20, respectively. The FMG moved toward the west twice during the 48 hour forecast, and as seen in



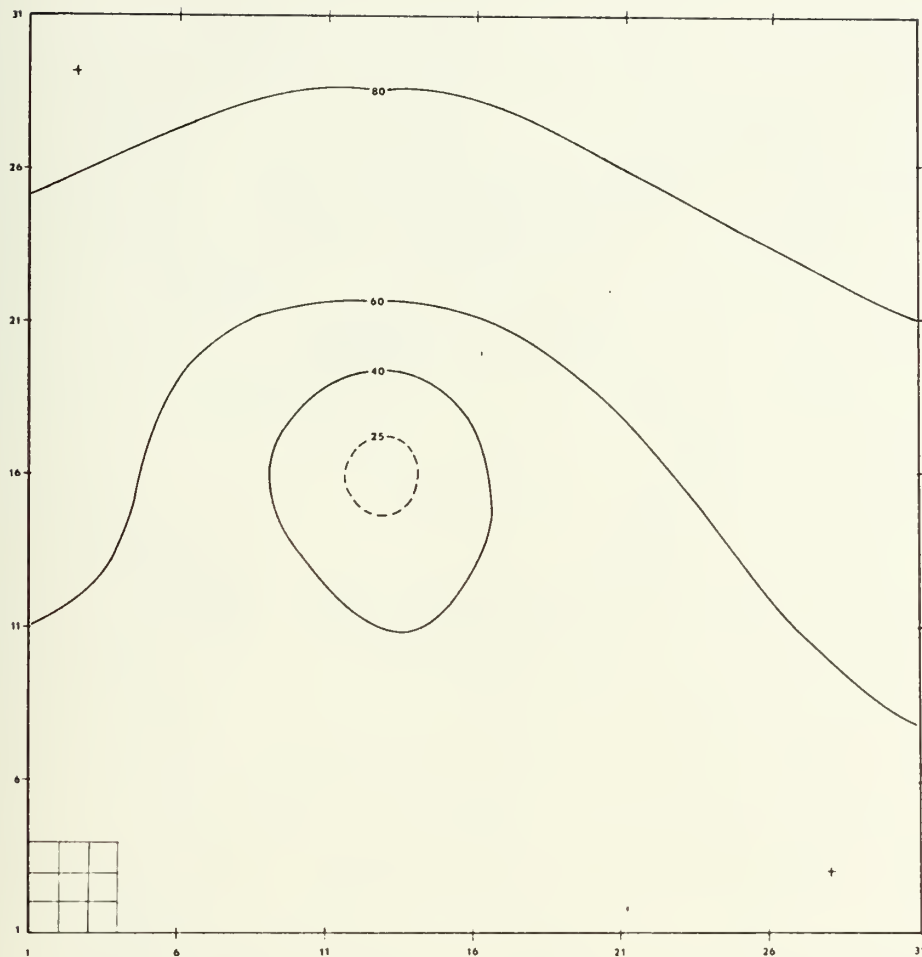


Fig. 21. Prediction of 850 mb heights (m) -1400m in the fine mesh after 48 hours. The FMG has moved twice during the forecast period. The FMG grid scale is indicated in the lower left corner.

Figure 21, the low center was again approaching the western side of the FMG. The large scale flow patterns were predicted quite similarly in both models.

Another example of the detail available in the FMG forecast is shown in Figure 22, the 48 hour vertical (pressure) velocity pattern at 700 mb in the FMG. The low center at 850 mb is denoted by the bold C, and areas of maximum





Fig. 22. Vertical (pressure) velocity ( $10^{-3} \text{ mb s}^{-1}$ ) in the FMG after 48 hours at 700 mb. The location of the 850 mb low center is denoted by the bold C, and the FMG grid scale is indicated in the lower left corner.

ascent are shaded. Although the heating is symmetric with respect to the low center (see Figure 19), there is a tendency for spiraling of the narrow bands of maximum ascent. The spatial increment of 36nm in the FMG prevents any very small scale details of the tropical storm simulation to be portrayed, but the overall pattern in Figure 22 is roughly





suggestive of observed data. If the model employed a parametric latent heating scheme dependent on vertical velocity, the shaded regions of ascent in Figure 22 might then be interpreted as cloud bands. The fact that such regions of ascent form in the model, without friction or a sophisticated latent heating scheme, suggests that such patterns may be independent of friction, and are probably linked to the dynamics of the flow itself.

Kinetic energy balance was also calculated for the CMG and FMG of the meshed model, and for the uniform coarse grid model, and is summarized in Table 5. As in the two-dimensional case, horizontal diffusion of momentum was employed in the FMG of the meshed model to suppress short wavelength computational noise, and therefore this region is the only one with dissipation included as a term in the balance. There are three separate balances because movement of the FMG required that a new balance be started at the completion of each move. Early in the prediction period (Table 5a), the diabatic heating had not yet caused the development of strong ascent regions in the FMG, and large dissipation governed the reduction of kinetic energy over this period in the meshed model. Generation of kinetic energy over this period was even less in the uniform coarse grid model, but because there was no dissipative mechanism or boundary flux, all the generation went to increase the total kinetic energy.



Table 5

a. Kinetic energy balance for meshed and uniform coarse grid models ( $10^{-2}$  joules  $\text{cm}^{-2}\text{day}^{-1}$ ) up to first move CMG time step 0-80.

Model	$\Delta\text{KE}$	Generation	Dissipation	Boundary flux
FMG	-3.6	+6.2	-8.1	-1.7
Meshed CMG	+3.2	+1.5	-	+1.7
Uniform grid	+4.5	+4.5	-	-

b. Kinetic energy balance for meshed and uniform coarse grid models up to second move CMG time step 80-160.

Model	$\Delta\text{KE}$	Generation	Dissipation	Boundary flux
FMG	+2.8	+13.4	-8.9	-1.7
Meshed CMG	+1.5	-0.2	-	+1.7
Uniform grid	+0.2	+0.2	-	-

c. Kinetic energy balance for meshed and uniform coarse grid models up to 48 hr CMG time step 160-240.

Model	$\Delta\text{KE}$	Generation	Dissipation	Boundary flux
FMG	+2.7	+21.3	-13.5	-5.1
Meshed CMG	-0.1	-5.2	-	+5.1
Uniform grid	+3.9	+3.9	-	-



In the intermediate period (Table 5b), the meshed system nearly restored the kinetic energy of the meshed system to the initial value, and the net generation was larger than the dissipation. Development of the regions of strong ascent as depicted in Figure 22 were established during this period, and the boundary flux across the interface remained approximately constant. Very little change occurred in the uniform grid model in this phase of the prediction period.

During the last phase of the prediction (Table 5c), the vertical motion pattern depicted in Figure 22 was fully established, and active over the entire phase in the meshed model, with accompanying large generation of kinetic energy in the FMG. The two-dimensional experiments previously indicated that the mutually determined boundary conditions allowed efficient interface transfer of kinetic energy, and this result was extended to the three-dimensional model as well. This may be seen in Table 5c, in that the greatly increased generation in the FMG did not cause excessive increase in the FMG kinetic energy, instead, FMG kinetic energy increased only slightly over the initial value, and the boundary flux increased with the increase in generation. The CMG apparently converted the kinetic energy to potential energy by gradually subsiding the warm upper level outflow from the interface over a large area.

Thermal balance in the two-dimensional test was obtained by performing all model computations in "double precision" on the IBM 360/67 at the Naval Postgraduate



School. This was necessary because the normal seven significant decimal places were not sufficient for balance, due to the magnitude of certain sums and forcing functions in the predictive equation (21). Increasing the decimal significance by a factor of two, however, nearly doubles the computer memory space requirements, and thus was impossible for the three-dimensional model. Behavior of accumulated heating and thermal boundary fluxes in time were examined, however, and these comparisons are portrayed in Figure 23. The accumulated

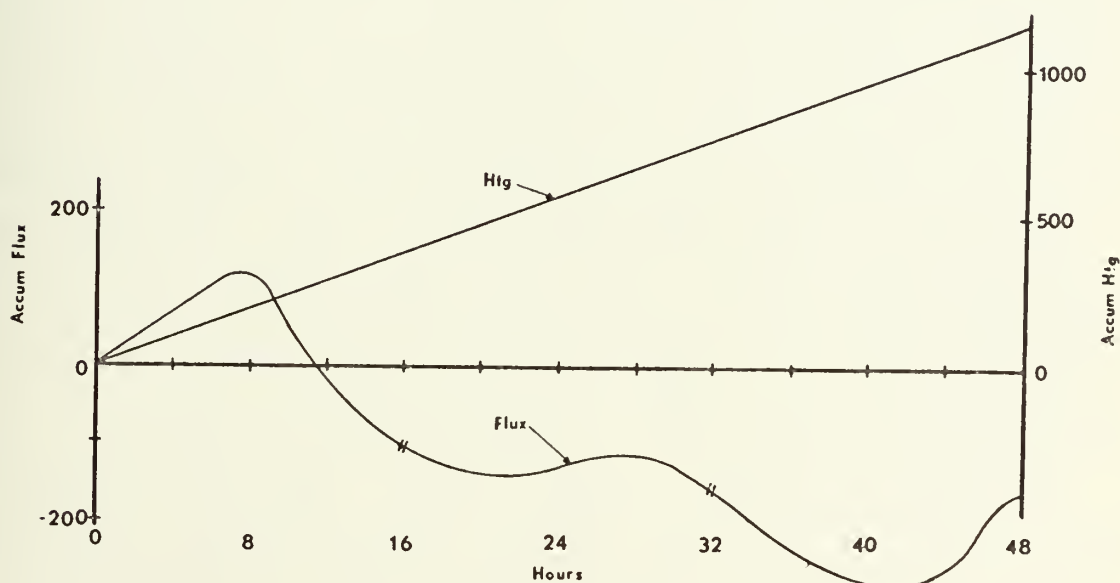


Fig. 23. Comparison of accumulated thermal boundary flux (left ordinate) with accumulated heating (right ordinate), in degrees of potential temperature integrated over the FMG. Compensatory radiative cooling in the CMG balanced the heating in the FMG at each vertical (pressure) level.

heating curve merely increases monotonically, since the heating rate was constant in time, but the accumulated thermal boundary flux curve behaved quite differently. In Figure 23, portions of the flux curve with positive





slope represent flux into the FMG, while those with negative slope indicate outward flux. The diagonal slashes on the flux curve denote the two movements of the FMG.

Two interesting features of the accumulated flux curve in Figure 23 are the initial flux into the FMG, and the oscillatory behavior of the flux for the remainder of the integration period. The initial flux into the FMG must be a result of adjustments between the scales in the interface region, since no ascent cell had been established at this early point in the integration, and the initial state was barotropic. In particular, the area averages assigned to the internal interface coincident points, and the external interface values which are determined by interpolation from CMG tendencies, may be quite different from the initial values, even after a few time steps. After approximately eight hours, the outward flux is monotonic, but oscillates with a period of about 16 hours. The reason for this oscillation is not clear, but it could be related to the FMG movement, which occurred each 16 hours for this test. Tests with different diabatic heating and mean zonal flow might help to indicate the cause of oscillation in the thermal boundary flux. Even though the flux behaved rather erratically, an important result was nevertheless established. That is, the mutually determined boundary specification in the three-dimensional model allowed both inward and outward thermal fluxes with no apparent computational difficulties.



#### D. SR TEST 2: A TEST OF INITIALIZATION AND SIMULATED FRONTAL DEVELOPMENT

In the previous tropical storm case, the FMG was large enough to completely encompass the region of large gradients and heating maximum. In the second test, to be described in this section, however, large gradients of wind and temperature were allowed at the interface. The objective of the frontal simulation test was twofold. First, a brief test of initialization procedures was desirable in a relatively smooth flow to perhaps suggest useful methods for real data initialization of the meshed system. Secondly, it was necessary for the sake of completeness of these tests of the meshing technique to study the behavior of the model in a more complex environment with a less idealized initial state. In this manner, some guidelines might be established as to size or other limitations of the FMG.

Deformation of an unstable baroclinic wave, closely resembling atmospheric frontogenesis, has been described by Hadfield (1970). This deformation resulted from horizontal shear in the mean wind field when a small amplitude disturbance was specified in the initial geopotential. This disturbance was independent of pressure, and superimposed on the basic zonal flow. The initial 1000 mb geopotential is given by

$$\phi_{1000} = f_o U \frac{L}{2\pi} \cos \left( \frac{2\pi x}{L} \right) \sin^2 \left( \frac{\pi y}{w} \right) \quad (27)$$



and the potential temperature by

$$\theta = f_o \frac{p(\frac{p_o}{p})^{R/c_p}}{R} \left[ \frac{\partial u}{\partial p} \left[ \frac{y}{2} + \frac{w}{4\pi} \sin \left( \frac{2\pi y}{w} \right) \right] + \theta_o + \frac{\partial \hat{\theta}}{\partial p} (p - p_o) \right] \quad (28)$$

where  $f_o = 10^{-4} \text{ s}^{-1}$ ,  $\partial u / \partial p = 0.05 \text{ ms}^{-1} \text{ mb}^{-1}$  and  $\frac{\partial \hat{\theta}}{\partial p}$ , the uniform lapse rate, was  $-0.376 \text{ K mb}^{-1}$ . The width, or north-south extent, of the domain is denoted by  $w$ , and the mean temperature  $\theta$ , was 300 K. The base pressure  $p_o$  was 1000 mb as in previous experiments. For this test of the meshed model, an additional term was included in (27) which caused the mean zonal flow at the middle level (550 mb) to be zero. This was done to eliminate the necessity of movement of the FMG, which was of no interest in this test. Thus there was strong easterly flow at lower levels, replaced by westerlies above 550 mb. Although this pattern was somewhat unrealistic for mid-latitude flow, the dynamics were unchanged, and more convenient for this test of the meshed model. Other details of this initial state are discussed by Hadfield (1970), and are of no further concern here.

Geopotential heights at the upper levels were then obtained with (23), and geostrophic winds were computed to complete the initialization. This simulated data was then the "real" data for the CMG and uniform coarse grid model, with the 550 mb geopotential heights and temperature pattern depicted in Figure 24. With the FMG located as indicated by the dotted outline in Figure 24, two tests of initialization



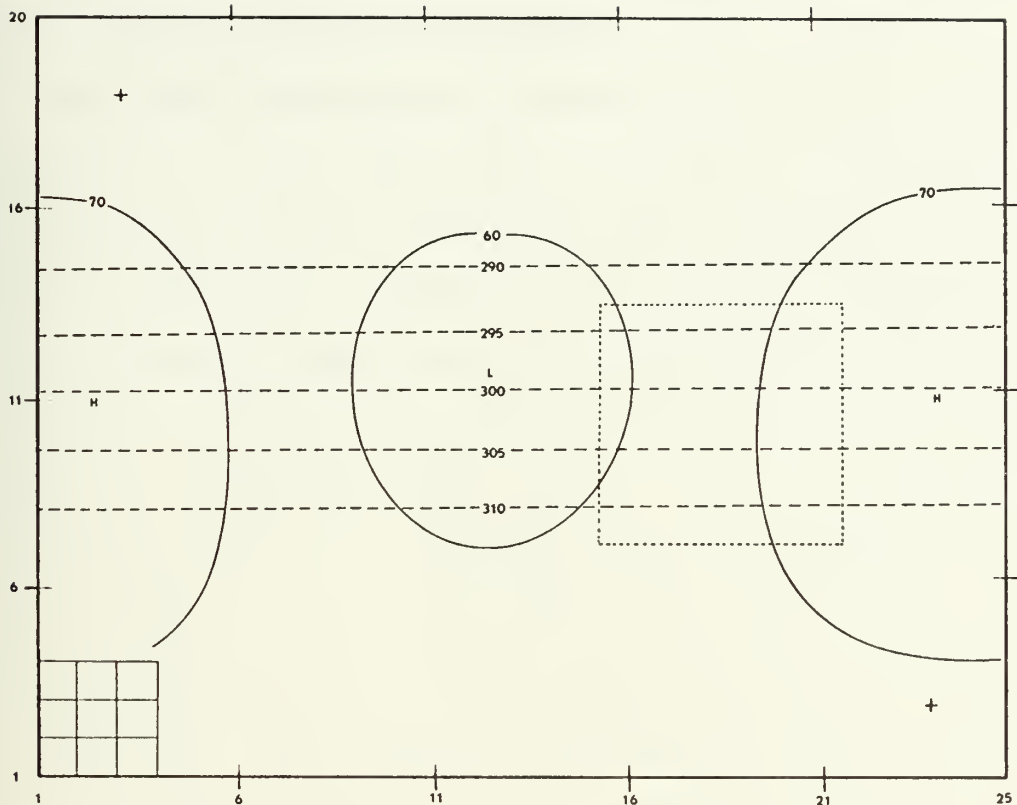


Fig. 24. Initial 550 mb height field - 5000 m (solid) and potential temperature (dashed). The position of the FMG for the initialization tests is indicated by the dotted outline.

were performed. The first initialization test involved direct linear interpolation of all dependent variables from the CMG values shown in Figure 24 onto the FMG. No attempt was made to perform diagnostics of any kind, and the integration commenced from this initial state in the FMG. Large amplitude, short wavelength modes were excited almost immediately and aliasing apparently led to non-linear computational instability in slightly over 24 hours. This result strongly indicated that interpolated values can probably not be used to initialize the FMG of a multi-level meshed model,





which utilizes the primitive equations. This is probably particularly true when strong, nonlinear gradients of dependent variables appear in the data.

The same interpolation procedure was carried out for the second test, except that only the winds were interpolated. The resulting FMG data then underwent a diagnostic phase after a consistent vertical motion pattern was obtained from (22). Balanced heights and hence temperatures were computed from (24), and with no other differences from the first case, this integration was carried out for 24 hours. The resulting forecast was qualitatively very similar to that obtained with the uniform coarse grid. This result suggested that this combination of interpolation and diagnostics may be useful for real data initialization in the meshed model. When the initial state shown in Figure 24 is integrated for several model days, the small amplitude disturbance results in deformation of the baroclinic zone. This deformation causes the formation of a frontal, or mid-latitude cyclone wave, with the initially small amplitude disturbance developing rapidly. Very strong winds develop, and in order to test the computational stability aspects of the meshing techniques in a complex environment, the FMG was located as depicted in Figure 25. The height and potential temperature fields portrayed in Figure 25, are those resulting after five model days (600 CMG time steps) in the uniform coarse grid model. These predicted values were then used as data to initialize the FMG. This test had two main objectives,



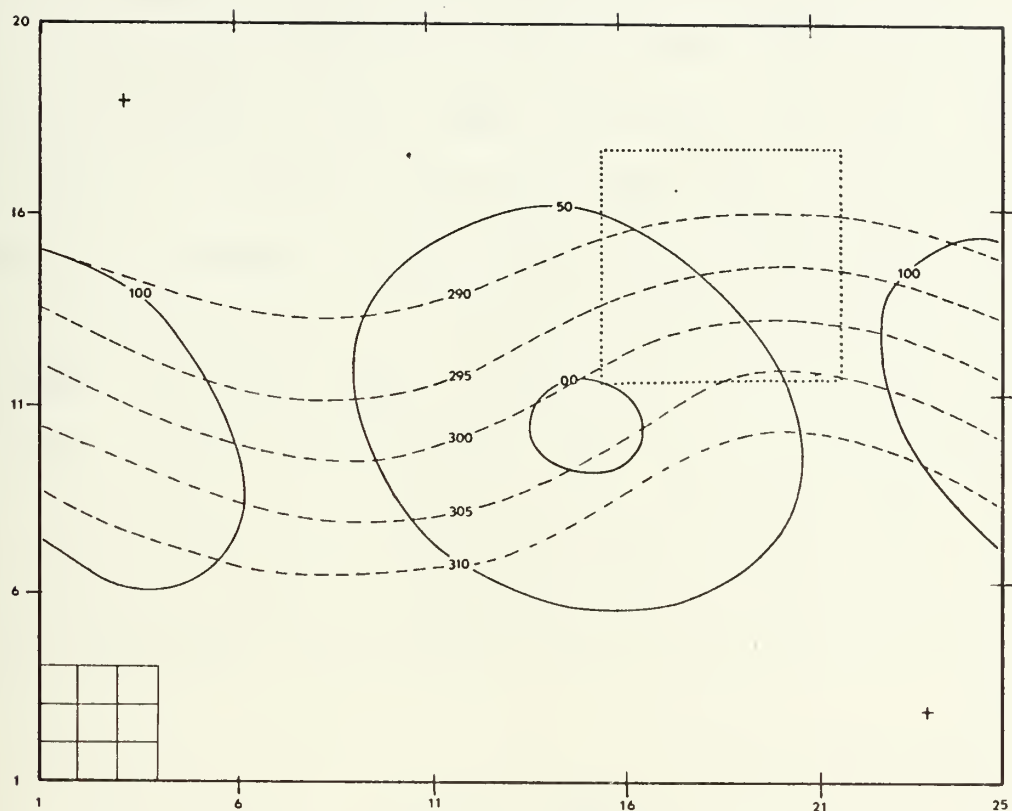


Fig. 25. Results of the uniform coarse grid for a five day forecast. The solid contours are 550 mb heights - 5000 m, and the dashed contours are isentropes. This forecast was the "initial" data for the meshed model test. See text for details.

the first of which was to subject the FMG interface to extremely large nonlinear gradients of all dependent variables to determine stability characteristics and other possible effects. Secondly, it was desired to study the solution in the FMG after the previously described initialization technique was utilized. In this case, however, the vertical motion patterns were fully developed, and the nonlinear terms in (24) would include the vertical advective quantities.



The same initialization procedure which proved the better of those tested in the less perturbed model atmosphere (Figure 24) was again employed for this test. The location of the FMG in Figure 25 was rather arbitrary, since not only did the regions of maximum potential temperature and height gradients not coincide, but the system was tilted toward the west at upper levels. It was obvious that the FMG depicted in Figure 25 was too small to model the cyclonic scale disturbance, but was nevertheless ideal for the test described here. Results of a one day forecast from the "initial" state shown in Figure 25 are depicted in Figure 26 for the

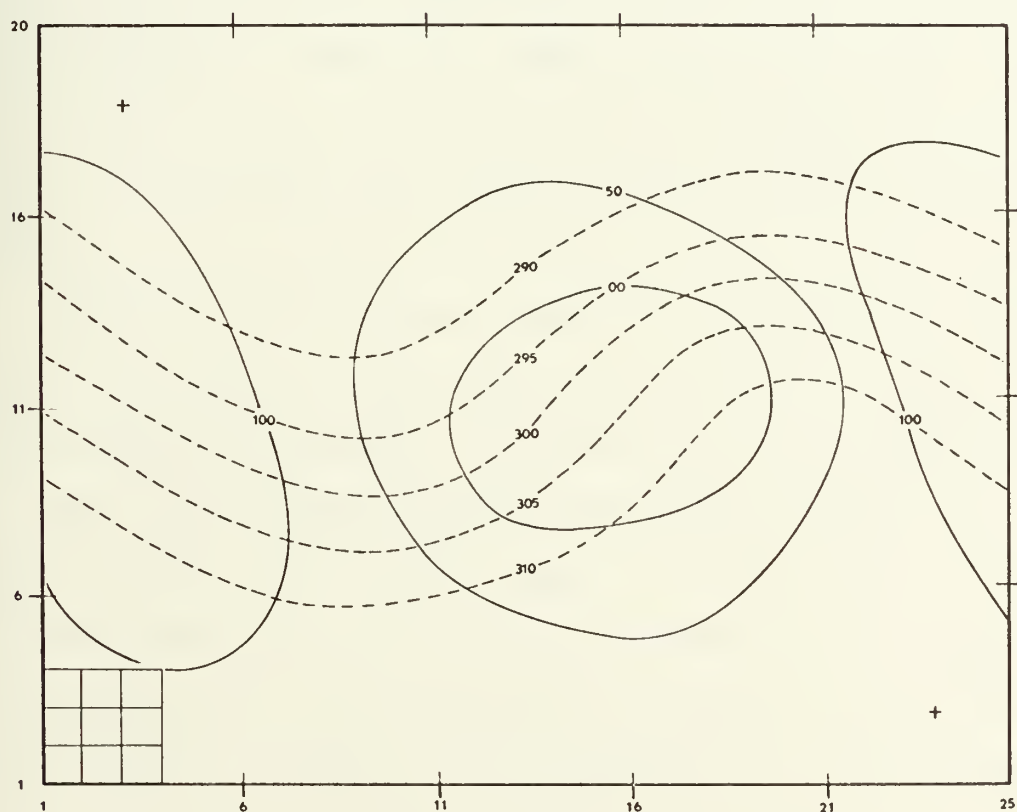


Fig. 26. Uniform coarse grid forecast for day six at 550mb. The solid contours are heights - 5000 m, and the dashed contours are isentropes.



uniform coarse grid model. The 550 mb height and potential temperature analyses at this time show that the gradients of both of these variables have increased, particularly on the "warm front" side. Strengthening of the gradients in this region was also noticed by Hadfield (1970) in similar experiments with a uniform grid model. The meshed model, on the other hand, produced a considerably different solution, as portrayed in Figure 27. Although deepening of the low was not as large, the 5100 m contour has closed, indicating enhanced development. As may be seen in Figure 27, the shape of both the height and potential temperature fields are different for the meshed model as compared to the uniform grid model result in Figure 26. This is not surprising, since phase speed errors are much less in the FMG, and development might be expected to be accelerated over that in the coarse grid.

Although the gradients have been strengthened in the FMG, it is difficult to argue that the solution is improved over the uniform grid result. At this point of the integration (6 days, 720 CMG time steps), the uniform coarse grid increment is still sufficiently small to resolve the gradients, and possible distortion at the interface due to phase speed differences may mask improvements resulting from the finer resolution in the FMG. To be assured of a more accurate solution for the frontal simulation, one would need to utilize an FMG several times larger than that depicted in Figure 27. Two important results of this test were that the mutually





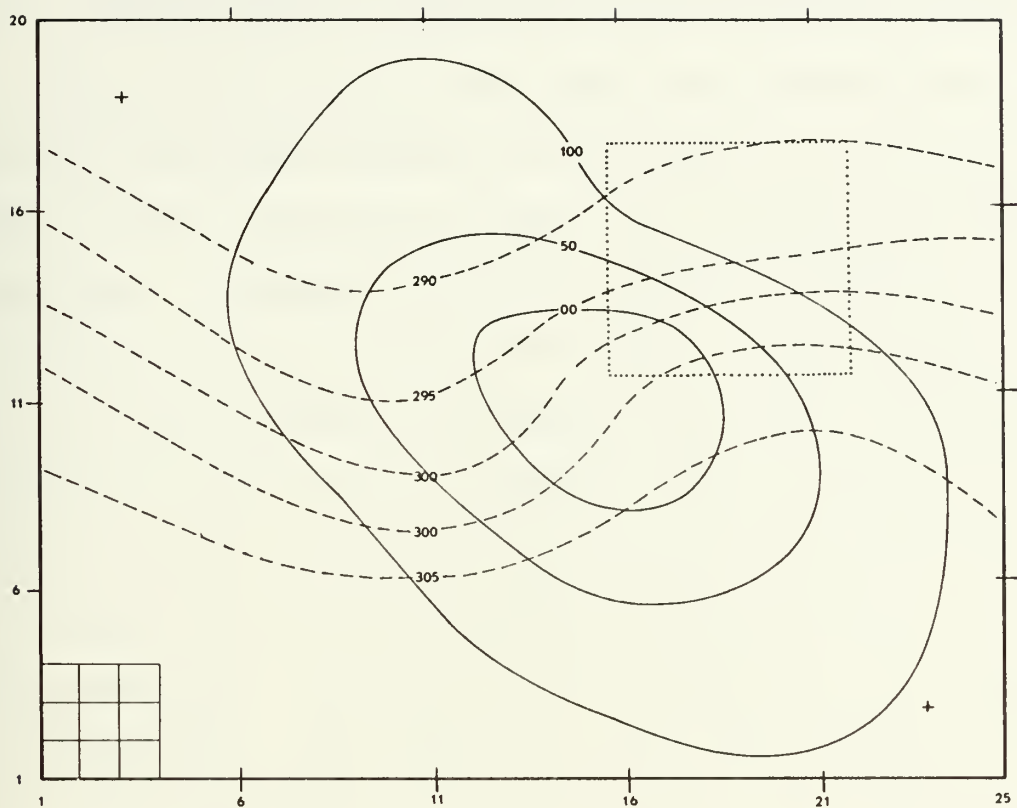


Fig. 27. Meshed model forecast for day six at 550 mb. The solid lines are heights - 5000 m, and the dashed contours are isotropes.

determined boundary specification retained the computational stability of the solution even in unfavorable situations, and that phase error was reduced in the FMG.



## VII. THE MR MODEL: A MULTIPLE GRID INCREMENT REDUCTION

Previous sections of this report have demonstrated the mutually determined boundary specification in several tests with a single reduction of grid scale between the coarse and fine grids. Although the abrupt increment change is computationally stable, and has been shown to yield results similar to those obtained on a uniform fine grid, one might argue heuristically that a gradual reduction in grid scale might prove less "traumatic" to the numerical solution. This might be particularly true in nonlinear systems with a large grid scale reduction. In the tests of the MR model described below, the same basic four-level primitive equation model discussed in previous sections was utilized.

### A. THE GRID AND MARCHING PROCESS

Several problems are encountered with multiple grid increment reduction if the mutually determined boundary specification is to be employed. One important limitation is that the ratio of reduction must be such that certain coincident points are maintained. As may be seen in the example depicted in Figure 28, each successive grid increment must decrease in the same ratio, or an integer multiple of the ratio, of the previous increment decrease. This is important in the movement of the FMG, in the boundary condition specification, and in the actual coding of the model. In Figure 28, the grids are labeled CMG (coarse mesh grid),



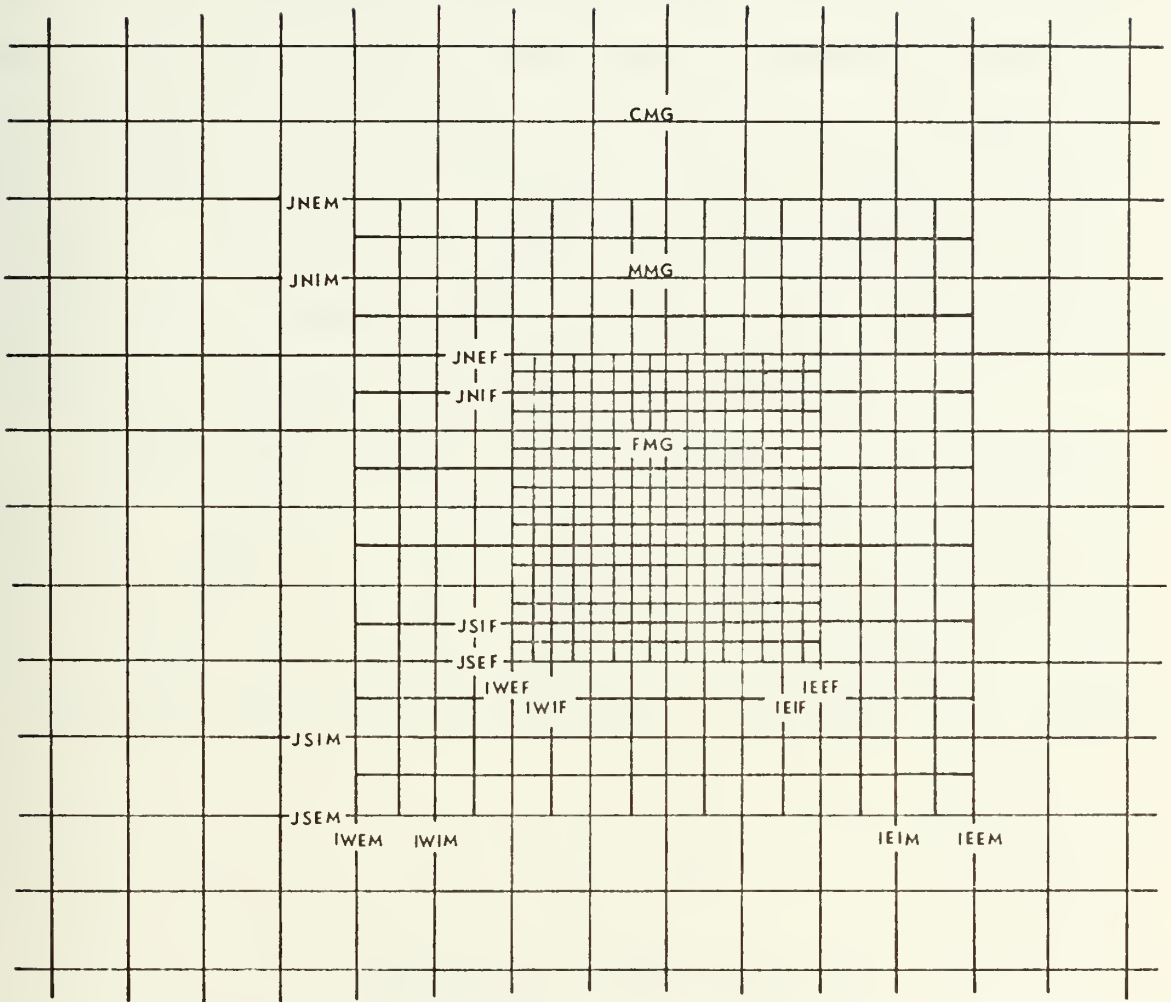


Fig. 28. An example of a horizontal level in the MR model. For this example, each of the smaller grids covers 8 x 8 increments of the next larger, and the spatial increment is reduced by one-half. See text for explanation of indices.

MMG (medium mesh grid), and FMG (fine mesh grid). The indicated index points are, as in the SR model, acronyms which indicate the location of either the MMG or the FMG. For example, IWEM, indicated I, West side, External interface and Medium grid. It should perhaps be emphasized that in the grid depicted in Figure 28, the acronymic indices ending with M are CMG indices, and those ending with F are MMG



indices. Thus the presence of the FMG is not "felt" by the CMG except indirectly through the MMG. Similarly, the CMG has no effect on the FMG other than by indirect effects transmitted through the MMG. In this manner, the MMG acts as a "buffer" between the largest and the smallest scale modeled. Thus regions of large nonlinear gradients may be modeled on the small scale desired, but the expense of having the entire FMG very small scale is eliminated.

The marching process for the MR model is more complex than the SR model, although it is analogous. Assuming that the first time step (which requires special attention) has been taken, the marching process may be described by referring to the schematic in Figure 29. By taking one centered

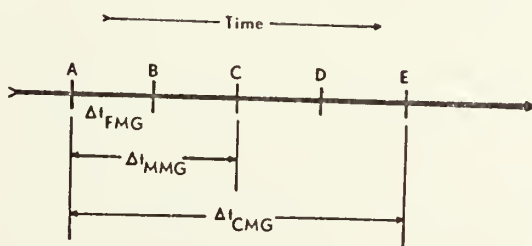


Fig. 29. A schematic to indicate the marching process in the MR model. The heavy line indicates any arbitrary position in time after the first time step, with the time between each point on the line representing one FMG time increment.

time step, the CMG solution may be raised from time level A to time level E. The tendencies around the MMG external





interface may then be determined by spatial and temporal interpolation. A centered time step in the MMG raises the solution in this grid from time level A to time level C, and the MMG external boundaries are updated from the previously determined CMG tendencies. Two centered time steps then need to be taken in the FMG to raise the solution in this grid from time level A to time level C. In this case, the external boundary values are determined from the MMG tendencies, and applied after each FMG time step. Finally, the internal interface values of the MMG are determined by the area average of the appropriate points in the FMG. The solutions in the two smaller grids are then raised from time level C to time level E by repeating the latter process. The final step in the marching process is to assign the CMG internal interface values by the appropriate area average in the MMG. The procedure for the first time step is quite similar, except that the first time step in each grid is forward in time, rather than centered.

Movement of the refined grids in the MR model is also analogous to that in the SR model. As the movement initiator (e.g., surface low pressure, maximum wind gradient, etc.) approaches the internal interface of the FMG, the FMG moves one MMG spatial increment in the appropriate direction. The MMG remains stationary within the CMG during this move, and leading and trailing edge values of the FMG at appropriate time levels are determined exactly as in the SR model. When the FMG approaches the edge of the MMG, the MMG moves one



CMG interval in the indicated direction, but during this move the FMG remains stationary. Thus the movement initiator for the MMG is independent of the atmospheric feature of interest, and depends only upon the location of the FMG. Leading and trailing edge values for the MMG are obtained in the usual manner after the movement, and all FMG location indices (i.e. IWEF, JSEF, etc.) must be redefined as the MMG "slides" under the stationary FMG.

#### B. TROPICAL STORM SIMULATION IN THE MR MODEL

One test similar to the tropical storm simulation in the SR model was performed utilizing the MR model. The major difference was that the mean zonal easterly flow was removed to eliminate the necessity of movement of the refined grids. The primary objectives of this test were to examine time and size requirements for the different grid scales, and to qualitatively compare the numerical results with those obtained with the SR model. It must, of course, be emphasized that removal of the zonal current will affect the solution, but similarities between the SR and MR solutions should still exist.

Initialization for the MR model was similar to that in the SR case. Geostrophic winds were analytically specified with (25), except that  $F(y) = 0$ . The divergence equation (24) was then solved for the heights first in the CMG, then in the MMG, and finally in the FMG. Boundary values for the MMG and FMG are obtained in an analogous manner as in the SR



model. The point vortex depicted in Figure 30 was, therefore, identical in amplitude and location to the one utilized for the SR test, but the actual values of the heights were modified because the mean zonal current was removed. The dotted outlines in Figure 30 indicate the position of the refined grids, with the FMG centered in the MMG, and also centered over the surface low center.

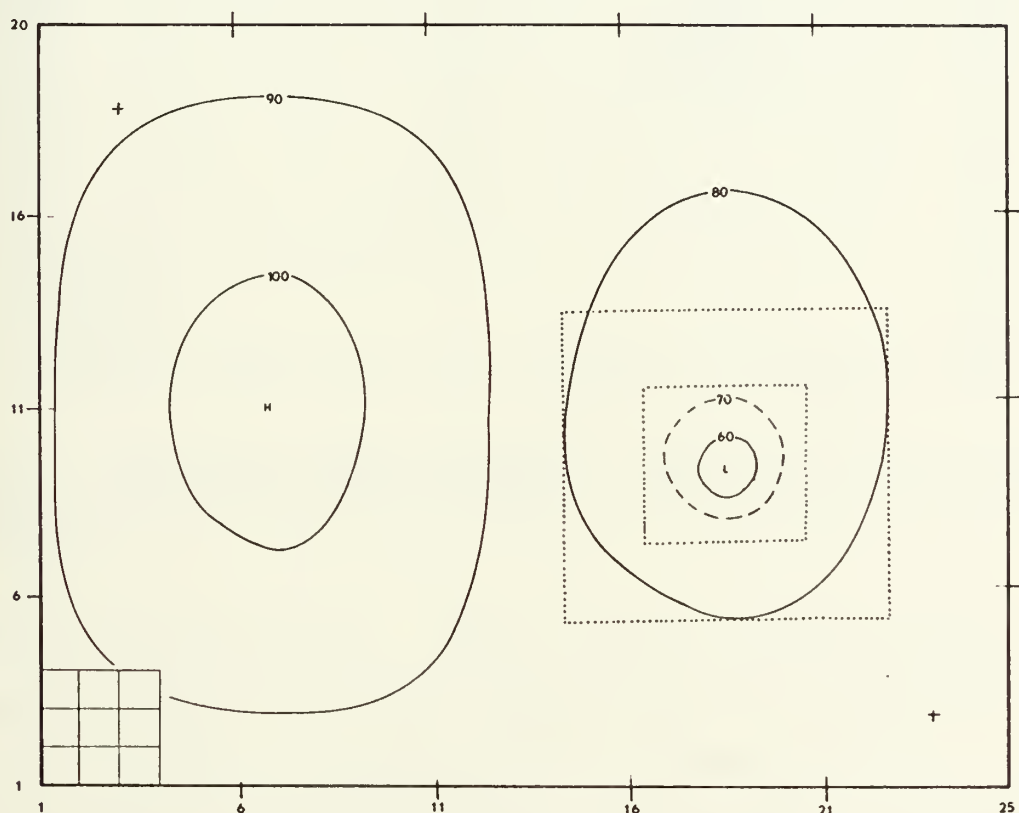


Fig. 30. Initial heights - 1400 m for the MR tropical storm simulation. The dotted outlines denote the location of the MMG (outer), and the FMG (inner). The CMG grid increment is indicated in the lower left corner.

The 850 mb height forecast for 48 hours is depicted in Figure 31 for the MR meshed system. As in the SR model, coincident CMG values in the MMG and FMG were replaced by those taken



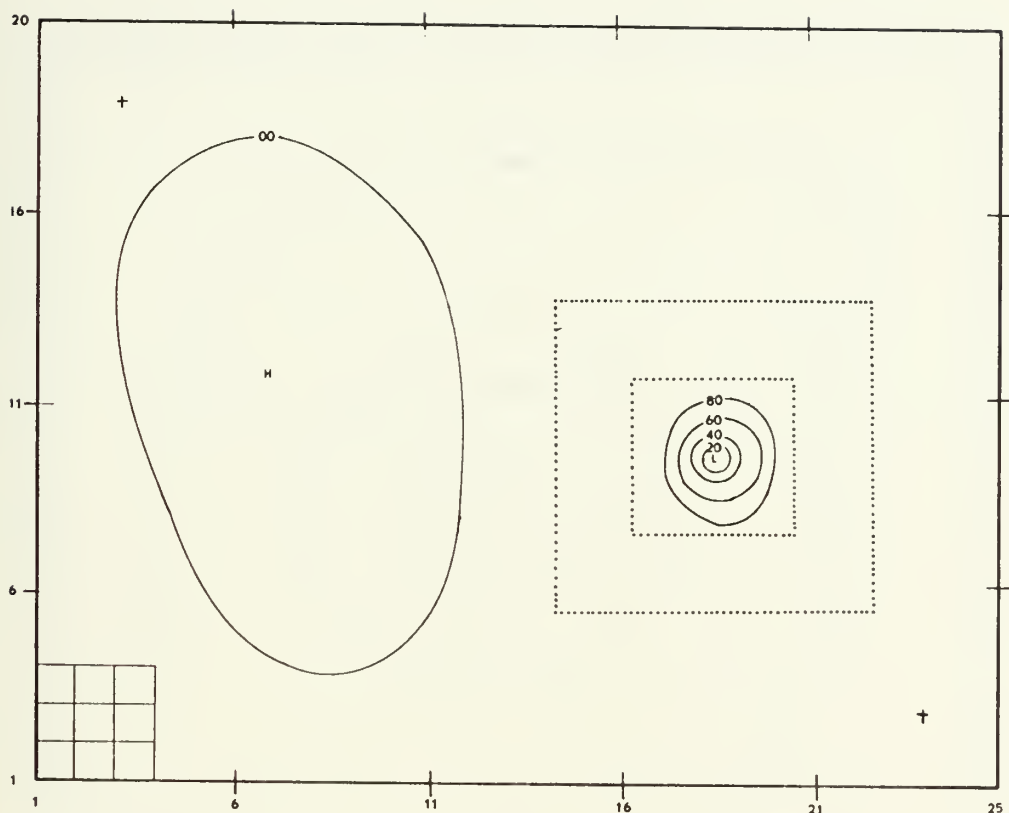


Fig. 31. Forecast 850 mb heights - 1400 m for the MR model. The location of the refined grids is indicated by the dotted outlines.

from the refined grids. The low center deepened approximately 40 meters, more than double that in the SR model. This was probably primarily due to the removal of the basic mean zonal flow since all other physical parameters were identical. This is further demonstrated by the 700 mb vertical motion pattern in the FMG depicted in Figure 32. In the SR model, the vertical motion tended to form narrow bands of ascent, while the ascent cell in the MR migrated to the low center. This suggested that formation of narrow areas of ascent may be related to the movement of the system





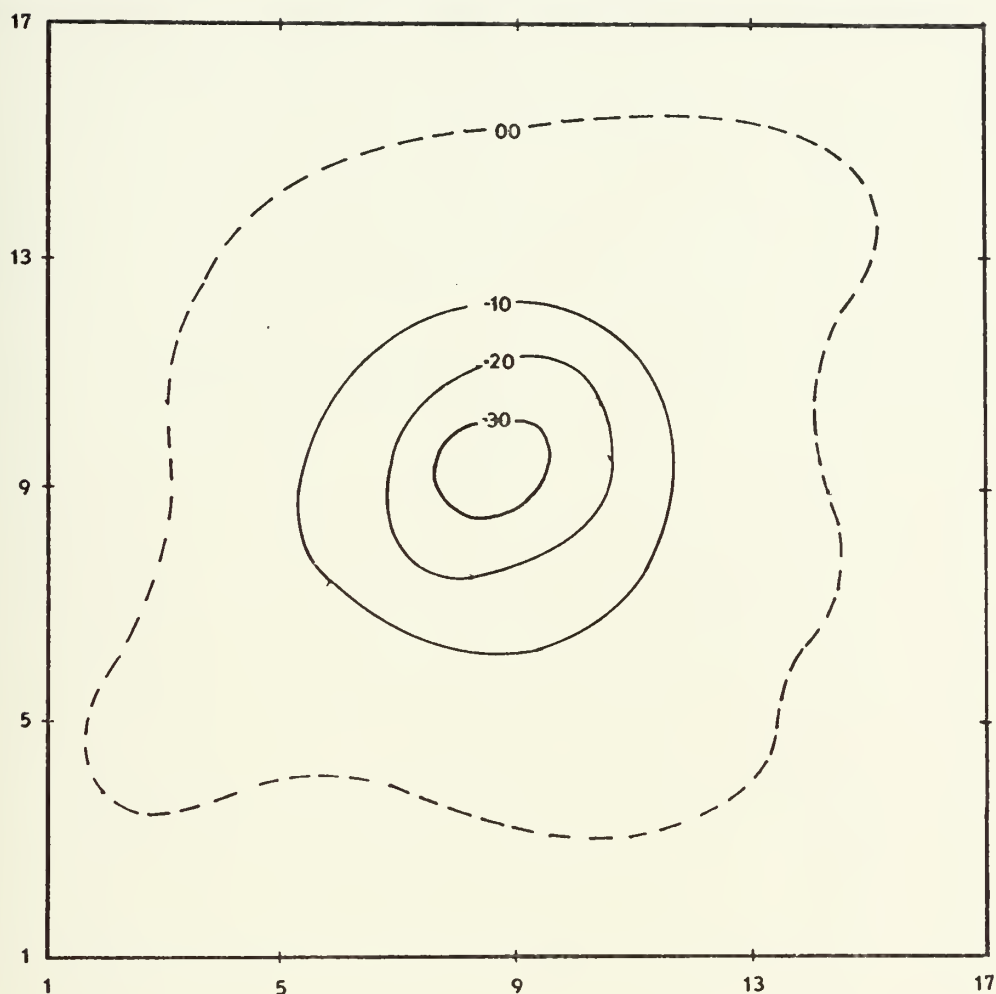


Fig. 32. Vertical motion pattern ( $\text{mb s}^{-1} \times 10^3$ ) after 48 hours at 700 mb for the FMG of the MR model.

through the surrounding environment. The main result of the MR test was to demonstrate that an improved detailed solution could be obtained with a gradual grid scale reduction, but at a fraction of the computer requirements. For the meshed MR model depicted in Figure 28, the computer memory requirement was approximately two-thirds, and the time requirement approximately one-half, that utilized in the  $p = 5$  SR model



utilized in earlier experiments. This was in spite of the fact that the MR model refined grid region covered  $8 \times 8$  CMG grid intervals, compared with  $6 \times 6$  for the SR version.



## VIII. SUMMARY

An important current problem in meteorology is the inclusion of small scale sources and sinks of energy in numerical models of the atmosphere. Related to this problem is the question of interactions between the planetary scale flow and the relatively small scale features which contribute the energy. Design of numerical models with uniform fine grids, which could possibly incorporate all these scales of motion, is currently quite impossible, due to computer time and memory limitations. In this paper, a possible solution to these important problems has been proposed. Different spatial increments were employed in the nested system, with the coarser grid increment an integer multiple of the finer increment. The inclusion, or nesting, of a finer resolution grid within a coarser one, allows small scale phenomena to be examined in detail without impractically large computer requirements.

The initial discussion of the nesting technique dealt with an analytic computational stability consideration and the appropriate related numerical tests of a simple linear equation, which was solved on both uniform and nested grid systems. Two unique aspects of the meshed grid system were the mutual interaction between the fine grid region and the surrounding coarse grid, due to the method of specifying the interface boundary values, and the fact that the



equation was integrated simultaneously in time on both grids. An approach due to Platzman (1954) which utilized the amplification matrix of the system of differential difference equations was used to show computational stability of the numerical solution when certain interface boundary specification was utilized. This analysis was valid when the same time increment was used in both grids, and the fine grid region remained stationary. Numerical solutions of the linear equation obtained with the nested grid system were shown to compare favorably with those resulting from integration in a uniform fine resolution grid. The mutually determined boundary specification was shown to be the only satisfactory one of those tested when centered space and time differencing was used. Analytical and numerical tests of other boundary specifications showed that these specifications were either computationally unstable, or produced inferior results.

Two important facets of the meshing technique also arose from the one-dimensional linear experiments. The first was the crucial fact that the computational stability of the mutually determined specification extended to the case where different time increments were used in each grid. This is particularly significant from the standpoint of obtaining a more accurate solution in the coarse grid, as well as most efficient utilization of computer time during the integration. Secondly, it was shown that movement of the fine grid region within the coarse grid had no apparent deleterious effect on the numerical solution. Subsequent numerical tests with





simple initial conditions, appropriate time increment in each grid, and movement of the fine grid to remain centered over a maximum gradient, again produced a numerical solution comparable to that obtained on a uniform fine grid.

Subsequent one-dimensional numerical tests with a non-linear system of equations demonstrated computational stability in more complex situations. An initial state which developed extremely sharp (eventually discontinuous) gradients was utilized to compare numerical solutions on uniform grids with those of the meshed system. The meshed grid solutions in this case were superior to those obtained on a uniform coarse grid, and nearly identical to those resulting when a uniform fine resolution grid was used.

Since the ultimate goal of this research was to develop a meshed three-dimensional primitive equation model, extension to a two-dimensional version was the next logical step. The two-dimensional model was a ten-level primitive equation model. The existence of internal and external gravity waves in such multi-level models was important in testing the meshing technique, because every interface boundary point may be an outflow boundary for either advective motions or gravity waves. The initial state for this test was a small scale heat source embedded in an otherwise undisturbed flow pattern, which stimulated the development of a convective type cell. Comparison of five-day forecasts showed the meshed system not only virtually reproduced the uniform grid solution inside the fine grid, but outside this region as well. This



result strongly suggested that the mutually determined specification allowed interaction between scales at the interface boundaries. This was further demonstrated in favorable comparisons of boundary fluxes of kinetic and thermal energy across the same spatial boundary in uniform fine and meshed systems. Certain computational devices were employed in the primitive equation models. The most significant was the utilization of horizontal momentum diffusion in the fine grid to suppress high frequency computational noise caused by truncation error differences between the grids, and slight inconsistencies in the boundary specifications. This was important because such short wavelength noise may eventually lead to nonlinear computational instability in primitive equation models.

All three-dimensional tests were performed utilizing a four-level primitive equation model. The fine grid covered approximately ten percent of the total spatial domain in the three-dimensional model. Initialization of data for these models was achieved by means of a divergence equation, which was derived from the difference form of the prediction equations. In all cases, winds were analytically specified, and balanced geopotential heights and temperatures were obtained by means of the divergence equation. The first test utilized an analytic initial state which simulated a tropical storm scale disturbance which was easily encompassed by the fine grid region. In this simulation, a circularly symmetrical vortex was embedded in the trough of a smooth wave in the



easterly flow. Heating was specified to roughly approximate the latent heat release inherent in such disturbances. Forecast results from a meshed model with a grid reduction of one-fifth in the fine grid were compared to those from a uniform coarse grid. No three-dimensional tests with uniform fine grids were possible because of computer limitations. The meshed model forecast depicted more detail of the storm simulation, and the movement of the vortex more closely agreed with the movement which would have resulted from purely advective processes. This test suggested that with a carefully specified initial state, and a fine grid which completely encompassed the region of interest, the meshed system yielded an improved solution.

To test the meshed model and the initialization scheme in a more complex situation, the second test employed the same grid, but included a frontal scale disturbance too large to be encompassed by the fine mesh region. The initial data for the meshed model was a numerical solution from a uniform coarse grid after several days of integration, and thus had a fully developed vertical motion pattern. The data were interpolated to the fine grid, and underwent a diagnostic phase with the previously derived divergence equation. Experiments showed that starting the integration without the diagnostic phase led to computational instability. An important point concerning this initialization was that the initial winds were not non-divergent, and all nonlinear terms, including vertical flux, were included in the divergence equation.



This test yielded two important results. First, the mutually determined boundary specification retained the computational stability of the numerical solution even in cases where strong, nonlinear gradients occurred at the interface. Secondly, the solution in the fine grid of the meshed model after one model day beyond the initial time appeared to enhance development over the entire spatial domain, and particularly in the fine grid system.

The final three-dimensional tests were performed with the same four-level primitive equation model, but with more than one reduction in grid scale. This was important because it allowed a small region of interest to be closely examined with a very fine grid, but without the computer time and memory expense which is inherent when the entire fine grid is extremely small scale. Thus, fairly active regions surrounding the disturbance, but some distance away, could still be modeled with finer resolution than the coarse grid, while the region of primary concern was modeled with even greater resolution. One test was performed with this meshed system, in which the initial state was a stationary vortex, identical to that in the single reduction tropical storm simulation, except the mean easterly flow was removed. Qualitative comparisons of two day forecasts between the single reduction model and the multiple reduction model demonstrated that improved solutions could be obtained with the multiple reduction model. These solutions compared





favorably with those obtained in the single reduction model, but utilized much less computer time and memory.

Many possible applications of the meshing technique discussed in this report exist. One of the most important has been suggested by several of the numerical experiments, namely forecasting the movement and development of tropical storms. It appears quite evident that if a fine mesh region was kept centered over a tropical storm in a prediction model, forecasts of these features would be improved. Another interesting related application would be experiments with tropical storm modification, in which the behavior of the storm system could be examined when heat is added at upper levels, for example. There are many other applications of meshed models, not only in meteorology, but also in other disciplines. When systems of equations are solved on finite grids, there is usually some limited portion of the solution domain that would be desirable to model with finer resolution than surrounding areas.



## APPENDIX A

### SEMI-DISCRETE AMPLIFICATION FOR MESHED AND UNIFORM GRID SYSTEMS

This appendix lists the semi-discrete amplification matrices discussed in section 2a. In each case, the CMG cyclic continuity is indicated by the first and last rows of the matrix. The mutually determined specification is retained for the meshed model at the inflow boundary (fourth row of each meshed model matrix), and the various outflow specifications listed in Table 1 are indicated at the outflow boundary (tenth row).

Matrix 1: Uniform grid with arbitrary external specification. This specification is stable for all cases (see Platzman 1954).

$$\begin{pmatrix} 0 & 1 & 0 & 0 & 0 & 0 & 0 & 0 & 0 & 0 & 0 & 0 & 0 & 0 \\ -1 & 0 & 1 & 0 & 0 & 0 & 0 & 0 & 0 & 0 & 0 & 0 & 0 & 0 \\ 0 & -1 & 0 & 1 & 0 & 0 & 0 & 0 & 0 & 0 & 0 & 0 & 0 & 0 \\ 0 & 0 & -1 & 0 & 1 & 0 & 0 & 0 & 0 & 0 & 0 & 0 & 0 & 0 \\ 0 & 0 & 0 & -1 & 0 & 1 & 0 & 0 & 0 & 0 & 0 & 0 & 0 & 0 \\ 0 & 0 & 0 & 0 & -1 & 0 & 1 & 0 & 0 & 0 & 0 & 0 & 0 & 0 \\ 0 & 0 & 0 & 0 & 0 & -1 & 0 & 1 & 0 & 0 & 0 & 0 & 0 & 0 \\ 0 & 0 & 0 & 0 & 0 & 0 & -1 & 0 & 1 & 0 & 0 & 0 & 0 & 0 \\ 0 & 0 & 0 & 0 & 0 & 0 & 0 & -1 & 0 & 1 & 0 & 0 & 0 & 0 \\ 0 & 0 & 0 & 0 & 0 & 0 & 0 & 0 & -1 & 0 & 1 & 0 & 0 & 0 \\ 0 & 0 & 0 & 0 & 0 & 0 & 0 & 0 & 0 & -1 & 0 & 1 & 0 & 0 \\ 0 & 0 & 0 & 0 & 0 & 0 & 0 & 0 & 0 & 0 & -1 & 0 & 1 & 0 \\ 0 & 0 & 0 & 0 & 0 & 0 & 0 & 0 & 0 & 0 & 0 & -1 & 0 & 1 \\ 0 & 0 & 0 & 0 & 0 & 0 & 0 & 0 & 0 & 0 & 0 & 0 & -1 & 0 \end{pmatrix}$$



Matrix 2: Meshed grid, mutually determined (Specification 1 in Table 1)

[illegible]

Matrix 3: Uniform grid, outflow constant in time (Specification 4 in Table 1)

[illegible]

Matrix 4: Meshed model, FMG outflow constant in time.

[illegible]



Matrix 5: Uniform grid, outflow value equal to adjacent interior value. (Specification 5 in Table 1)

[illegible]

Matrix 6: Meshed grid, FMG outflow value equal to adjacent interior FMG value.

[illegible]





Matrix 7: Uniform grid, outflow value equal to second adjacent interior point value (Specification 6 in Table 1).

[illegible]

Matrix 8: Meshed grid, FMG outflow value equal to second adjacent interior point value.

[illegible]



Matrix 9: Uniform grid, outflow value determined by linear extrapolation from two adjacent interior points (Specification 7 in Table 1).

[illegible]

Matrix 10. Meshed grid, FMG outflow determined by linear extrapolation from two adjacent interior FMG points.

[illegible]



## LIST OF REFERENCES

1. Anthes, R. A., 1970: Numerical experiments with a two-dimensional horizontal variable grid. Mon. Wea. Rev., 98, 810-822.
2. Arakawa, A., 1966: Computational design for long term numerical integration of the equations of fluid motion: two-dimensional incompressible flow, Part 1, J. Comp. Phys., 1, 119-143.
3. Birchfield, G. E., 1960: Numerical prediction of hurricane movement with the use of a fine grid. J. Meteor., 17, 404-414.
4. Bushby, F. H., 1968: Further developments of a model for forecasting rain and weather. Proc. WMO/IUGG Symp., Tokyo, II, 75-84.
5. \_\_\_\_\_, and M. S. Timpson, 1967: A 10-level atmospheric model and frontal rain. Quart. J. Roy. Met. Soc., 93, 1-17.
6. Charney, J. G., 1960: Integration of the primitive and balance equations. Proc. Int. Symp. Num. Wea. Pred., Tokyo, 131-152.
7. \_\_\_\_\_, R. Fjortoft and J. von Neumann, 1950: Numerical integration of the barotropic vorticity equation. Tellus, 4, 237-254.
8. Ciment, M., 1971: Stable difference schemes with uneven mesh spacings. Math. Comp., 25, 219-227.
9. Courant, R., K. Friedrichs, and H. Lewy, 1928: Uber die partiellen Differenzengleichungen der mathematischen Physik. Math. Ann., 100, 32-74.
10. Elsberry, R. L., and E. J. Harrison, Jr., 1971: Height and kinetic energy oscillations in a limited region prediction model. Mon. Wea. Rev., 99, 883-888.
11. \_\_\_\_\_, 1972: Effects of parameterization of latent heating in a tropical prediction model. J. Appl. Meteor., 11, 255-267.
12. Estoque, M. A., 1962: Vertical and radial motions in a tropical cyclone, Tellus, 14, 394-402.



13. Gerrity, J. P., Jr. and R. D. McPherson, 1969: Development of a limited area fine-mesh prediction model. Mon. Wea. Rev., 97, 665-669.
14. Hadfield, R. R., 1970: A study of atmospheric frontogenesis with the primitive equations. M. S. Thesis, Naval Postgraduate School, Monterey, Ca., 58 pp.
15. Harrison, E. J., Jr., 1969: Experiments with a primitive equation model designed for tropical application. M. S. Thesis, Naval Postgraduate School, Monterey, Ca., 60 pp.
16. Hill, G. E., 1968: Grid telescoping in numerical weather prediction. J. Appl. Meteor., 7, 29-38.
17. Holton, J. R., 1971: A diagnostic model for equatorial wave disturbances: The role of vertical shear of the mean zonal wind. J. Atm. Sci., 1, 55-64.
18. Howcroft, J. G., 1966: Fine mesh limited area forecasting. Tech. Rep. 188, U. S. Air Weather Service, Scott AFB, 71-75.
19. Kuo, H. L., 1965: On the formation and intensification of tropical cyclones through latent heat release by cumulus convection. J. Atmos. Sci., 22, 40-63.
20. Kurihara, Y., 1965: On the use of implicit and iterative methods for the time integration of the wave equation. Mon. Wea. Rev., 93, 33-45.
21. Nitta, T., 1962: The outflow boundary conditions in numerical time integration of advective equations. J. Meteor. Soc. Jap., 40, 13-24.
22. Ookochi, Y., 1972: A computational scheme for the nesting fine mesh in the primitive equation model. J. Meteor. Soc. Jap., 50, 37-47.
23. Osher, S., 1970: Mesh refinements for the heat equation. SIAM J. Num. Anal., 2, 199-205.
24. Phillips, N. A., 1972: On the strategy of combining coarse and fine grid meshes in numerical weather prediction, to appear in J. Appl. Meteor.
25. Platzman, G. W., 1954: The computational stability of boundary conditions in numerical integration of the vorticity equation. Arch. Met. Geophys. Bioklimatol., 7, 29-40.





26. Rousseau, D., 1968: Experience preliminaire a l'elaboration d'un modele numerique de prevision regional. Ministere des Transports, Secretariat General a l'Aviation Civile, Notes de l'establissement d'etudes et de recherches meteorologiques, 25 pp.
27. Shapiro, M. A., and J. J. O'Brien, 1970: Boundary conditions for fine-mesh limited-area forecasts. J. Appl. Meteor., 9, 345-349.
28. Shuman, F. G., and J. B. Hovermale, 1968: An operational six-layer primitive equation model. J. Appl. Meteor., 7, 525-546.
29. Sundqvist H., and G. Veronis, 1970: A simple finite difference grid with non-constant intervals. Tellus, 22, 26-31.
30. Wang, H. H., and P. Halpern, 1970: Experiments with a regional fine-mesh prediction model. J. Appl. Meteor., 9, 545-553.
31. Williams, R. T., and A. M. Hori, 1970: Formation of hydraulic jumps in a rotating system. J. Geophys. Res., 15, 2813-2821.
32. Wurtele, M. G., 1961: On the problem of truncation error. Tellus, 3, 279-391.
33. Yamasaki, M., 1968: Numerical simulation of tropical cyclone development with the use of primitive equations. J. Meteor. Soc. Jap., 46, 178-201.



# INITIAL DISTRIBUTION LIST

	No. Copies
1. Defense Documentation Center Cameron Station Alexandria, Virginia 22314	2
2. Library, Code 0212 Naval Postgraduate School Monterey, California 93940	2
3. Dr. Russell L. Elsberry Department of Meteorology (51) Naval Postgraduate School Monterey, California 93940	8
4. LCDR E. J. Harrison, Jr. FLEWEACEN Box 12 COMNAVMARIANAS FPO San Francisco, California 96630	3
5. Naval Weather Service Command Washington Navy Yard Washington, D. C. 20390	1
6. Dr. Roger T. Williams Department of Meteorology (51) Naval Postgraduate School Monterey, California 93940	1
7. Dr. Frank D. Faulkner Department of Mathematics Naval Postgraduate School Monterey, California 93940	1
8. Dr. K. E. Woehler Department of Physics Naval Postgraduate School Monterey, California 93940	1
9. Dr. M. G. Wurtele Department of Meteorology U.C.L.A. Los Angeles, California 90024	1
10. Commanding Officer Fleet Numerical Weather Central Naval Postgraduate School Monterey, California 93940	1



11. Director, Naval Research Laboratory 1  
Attn: Tech. Services Info Officer  
Washington, D. C. 20390
12. Department of Meteorology 1  
Code 51  
Naval Postgraduate School  
Monterey, California 93940
13. Department of Oceanography 1  
Code 58  
Naval Postgraduate School  
Monterey, California 93940
14. American Meteorological Society 1  
45 Beacon Street  
Boston, Massachusetts 02128
15. Office of Naval Research 1  
Department of the Navy  
Washington, D. C. 20360
16. Dr. Fred Shuman, Director 1  
National Meteorological Center  
NOAA  
Suitland, Maryland 20390
17. Dr. J. Smagorinsky, Director 1  
Geophysical Fluid Dynamics Laboratory  
Princeton University  
Princeton, New Jersey 08540
18. Professor N. A. Phillips 1  
54-1422  
M. I. T.  
Cambridge, Massachusetts 02139
19. Dr. A. Arakawa 1  
Department of Meteorology  
U.C.L.A.  
Los Angeles, California 90024
20. Dr. Stanley Rosenthal 1  
National Hurricane Research Laboratory  
P.O. Box 8265, University of Miami Branch  
Coral Gables, Florida 33124
21. Dr. Banner Miller 1  
National Hurricane Research Laboratory  
P.O. Box 8265, University of Miami Branch  
Coral Gables, Florida 33124



22. Dr. Robert L. Haney  
Department of Meteorology (51)  
Naval Postgraduate School  
Monterey, California 93940

1





## DOCUMENT CONTROL DATA - R &amp; D

(Security classification of title, body of abstract and indexing annotation must be entered when the overall report is classified)

1. ORIGINATING ACTIVITY (Corporate author) Naval Postgraduate School Monterey, California 93940		2a. REPORT SECURITY CLASSIFICATION Unclassified	
		2b. GROUP	
3. REPORT TITLE A Method for Incorporating Nested Finite Grids in the Solution of Systems of Geophysical Equations			
4. DESCRIPTIVE NOTES (Type of report and inclusive dates) Doctor of Philosophy Thesis; June 1972			
5. AUTHOR(S) (First name, middle initial, last name) Edward J. Harrison, Jr.			
6. REPORT DATE June 1972		7a. TOTAL NO. OF PAGES 124	7b. NO. OF REFS 33
8a. CONTRACT OR GRANT NO.		9a. ORIGINATOR'S REPORT NUMBER(S)	
b. PROJECT NO.			
c.		9b. OTHER REPORT NO(S) (Any other numbers that may be assigned this report)	
d.			
10. DISTRIBUTION STATEMENT Approved for public release; distribution unlimited.			
11. SUPPLEMENTARY NOTES		12. SPONSORING MILITARY ACTIVITY Naval Postgraduate School Monterey, California 93940	

## 13. ABSTRACT

A numerical technique with simultaneous time integration of a meshed grid system is proposed, in which the fine mesh region is able to move within the coarse grid. The interface boundary conditions employed are shown analytically to be the only stable specification of those tested for a simple linear case. Numerical solutions using the meshed system are compared with those from uniform coarse and fine grids. One important criterion is that the solution within the fine mesh region of the meshed grid must have nearly the same accuracy as in a system which uses a fine mesh everywhere. The technique is applied to a two-dimensional (y,p) ten-level primitive equation model. Behavior of the meshed model is examined in experiments in which a small scale heat source is imbedded within an undisturbed zonal flow pattern. Energy boundary fluxes across the interface in the meshed system are shown to compare favorably with those in a uniform fine mesh grid. Three-dimensional (x,y,p) versions of the primitive equation model with single and multiple grid reductions are also examined. Simulated small scale disturbances are used to compare the meshed model solutions with those obtained on a uniform grid. Future applications of the meshing technique are suggested, such as in tropical storm research and general circulation models of the atmosphere and ocean.



KEY WORDS	LINK A		LINK B		LINK C	
	ROLE	WT	ROLE	WT	ROLE	WT
Meshed grids						
Nested grids						
Grid refinement						
Primitive equation model						
Numerical weather prediction						



28 MAY 75

S107121

Thesis  
H29325 Harrison  
c.1

134787

A method for incorporating nested finite grids in the solution of systems of geophysical equations.

20 MAY 80

S107121

Thesis  
H29325 Harrison  
c.1

134787

A method for incorporating nested finite grids in the solution of systems of geophysical equations.

thesH29325

A method for incorporating nested finite



3 2768 002 08247 1

DUDLEY KNOX LIBRARY